A Multicarrier-CDMA Space–Time Receiver With Full-Interference-Suppression Capabilities

Besma Smida, *Member, IEEE*, Sofiène Affes, *Senior Member, IEEE*,
Kamal Jamaoui, and Paul Mermelstein, *Fellow, IEEE*

Abstract—This paper proposes a low-complexity multicarrier-code-division-multiple-access (MC-CDMA) space–time receiver with full-interference-suppression capabilities. First, we derive a complete model of the interference which takes into account multiple-access, intersymbol, and intercarrier interferences. Based on this model, we introduce a new multicarrier-interference-subspace-rejection (MC-ISR) receiver and analyze its performance in an unknown time-varying Rayleigh channel with multipath, carrier offset, and cross correlation between subcarrier channels. We also propose a realistic implementation of this receiver, which includes an efficient strategy for carrier-offset recovery in a multicarrier- and multiuser-detection scheme. In addition, based on the Gaussian assumption, we derive a link-/system-level performance analysis of the MC-ISR over the two MC-CDMA air-interface configurations, which are the multitone CDMA and the multicarrier direct-sequence CDMA, and validate it by simulations. The gains in the throughput, which are attainable by the MC-ISR, are significant and evaluated in this paper as functions of the air-interface configuration, the number of subcarriers, and the modulation order.

Index Terms—Antenna arrays, code division multiple access (CDMA), intercarrier-interference (ICI) suppression, interference rejection, multicarrier direct-sequence CDMA (MC-DS-CDMA), multicarrier systems, multitone (MT)-CDMA, multiuser detection.

I. INTRODUCTION

CODE DIVISION multiple access (CDMA) is the multiple-access technology used in third-generation cellular systems. It is predicted that future wireless systems will be operating mainly on burst data services carrying multimedia traffic including voice, data, image, and video. The need to support such a great amount of high-rate and burst-type traffic in wireless channels poses serious challenges to the current CDMA air interface. Techniques that could effectively enhance the overall bandwidth efficiency will be vital in facilitating CDMA technological evolution toward the next generation.

Multicarrier modulation combined with CDMA, usually referred to as multicarrier CDMA (MC-CDMA), has received considerable attention because it has high spectral efficiency. Various MC-CDMA schemes have been proposed in the literature. They can be divided into two categories: One combines multicarrier modulation with frequency-domain spreading, and the other transmits several direct-sequence CDMA (DS-CDMA) waveforms in parallel with the spreading operation performed in time. The transmitter proposed here belongs to the second group (the study of the first group is beyond the scope of this paper). In the second group, the transceivers can be divided into MC-DS-CDMA and multitone (MT)-CDMA, with the difference between the two being the subcarrier frequency separation. They can be unified in a family of generalized MC-DS-CDMA transceivers, defined in [1], using a range of frequency spacings, parameterized by λ, between two adjacent subcarriers. In this paper, we adopt this general view and simply refer to it as the MC-CDMA in the remainder of the paper, unless otherwise required.

Although the MC-CDMA systems are promising, challenges remain before they can achieve their full potential. One of the major obstacles in detecting the MC-CDMA signals is interference. The multiple-access interference (MAI) and the intersymbol interference (ISI), which are inherited from the conventional DS-CDMA, likewise affect the performance of the MC-CDMA systems. In addition, MC-CDMA capacity is limited by the intercarrier interference (ICI) due to the use of multicarrier modulation. Indeed, imperfect frequency down-conversion due to the instability of local oscillators combined with the multipath effect destroys the subcarriers' orthogonality, thereby causing the ICI [1], [2].

Since the MC-CDMA systems also contain a DS-CDMA component, traditional multiuser-detection techniques can be performed on each carrier with some form of adaptation. A variety of multiuser receivers have been investigated for the MC-CDMA systems, such as minimum mean square error (MMSE), [3], successive interference cancellation [4], parallel interference cancellation [5], [6], MMSE/decorellator [7], and subspace multiuser detection [8], [9]. Most of these receivers have focused on the MAI while ignoring the ICI. In addition, important system-design issues, such as carrier-frequency-offset recovery (CFOR), have often been neglected. In
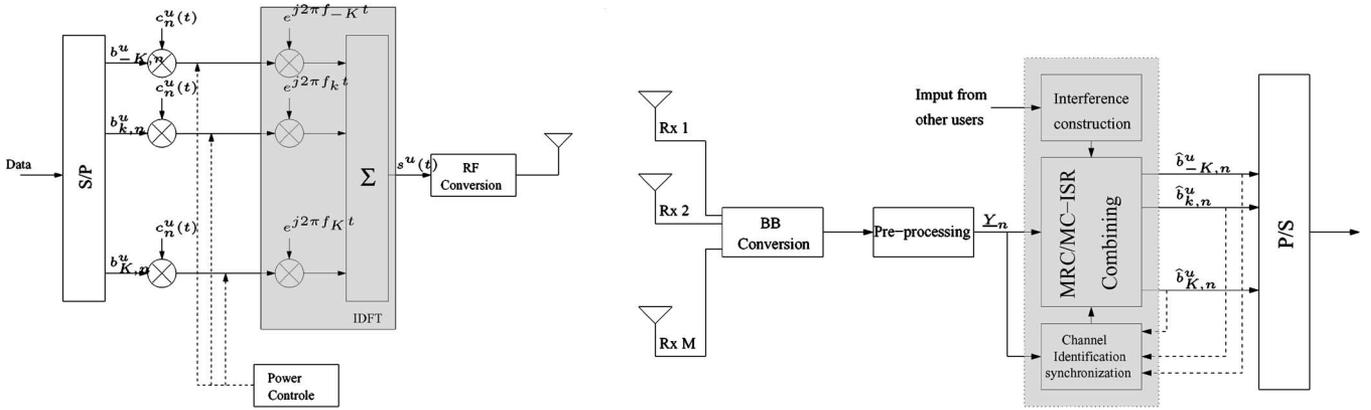
Fig. 1.   Block diagram of the MC-CDMA transmitter and receiver (pulse-shape filtering is implemented at both transceiver ends).

multiuser detection, the CFO of one user not only degrades the detection of that user itself but also makes the receiver based on the ideal carrier-frequency acquisition no longer optimal, thus degrading the detection of the other users [10]. An alternative multiuser-detection technique, denoted as interference subspace rejection (ISR), has been proposed for the DS-CDMA [11]. This technique offers different modes. Each mode characterizes the interference vector in a different way and, accordingly, suppresses it. The flexibility and the robustness inherent to the ISR make its exploitation in multicarrier systems of great interest.

In this paper, a low-complexity multicarrier space–time receiver is developed, which mitigates the full interference effect while confronting wireless-channel impairments. First, we derive a complete model of the interference, which takes into account the MAI, the ISI, and the ICI in a multipath fading channel with a timing and frequency mismatch. Based on this model, we propose a new multicarrier-ISR (MC-ISR) receiver with full-interference-suppression capabilities. We incorporate the least complex and the more practical ISR interference-rejection mode to simultaneously suppress the MAI, the ISI, and the ICI at the signal-combining step. We also propose a realistic implementation of the new MC-ISR receiver, which includes an efficient strategy for carrier-offset recovery in a multicarrier- and multiuser-detection scheme.

Furthermore, the assessment of the new MC-ISR receiver is oriented toward an implementation in a future real-world wireless system. We, hence, assume the correlated Rayleigh channels across the subcarriers. Indeed, fading characteristics among the subcarriers are highly correlated due to insufficient frequency separation between the subcarriers. Additionally, we analyze the performance of the MC-ISR using realistic link-level-simulation setups that take into account time and frequency mismatch, imperfect power control, channel-identification errors, etc. As another contribution in this paper, we also derive a link-/system-level performance analysis of the MC-ISR based on the Gaussian assumption (GA). The GA is based on the observation that the interference is approximately Gaussian. Simulation results confirm the match of the GA under practical conditions and the net advantage of the full-interference-suppression capabilities of the MC-ISR. They also show that for both differential binary-phase-shift-

keying (DBPSK) and differential eight-level phase-shift-keying (D8PSK) modulations, the MT-CDMA has the best link-level performance compared with the MC-DS-CDMA and has the highest throughput. With two receiving antennas and nine MT-CDMA subcarriers in a 5-MHz bandwidth, the MC-ISR provides about 4320 kb/s at low mobility for the DBPSK, i.e., an increase of 115% in the throughput over a DS-CDMA system with the maximum ratio combining (MRC).

The rest of the paper is organized as follows. Section II gives a detailed description of the transmitter, the channel model, and the complete interference model for an MC-CDMA air interface. In Section III, we introduce the new MC-ISR receiver with full interference suppression and derive a link-/system-level performance analysis based on the GA. In Section IV, we analyze the performance of this new receiver for the MC-DS-CDMA and MT-CDMA configurations. Finally, we conclude in Section V.

II. DATA MODEL AND ASSUMPTIONS

A. Transmitter

We consider the uplink of an asynchronous multicellular MC-CDMA system with C incell active users. For the sake of simplicity, we assume that all users use the same subcarriers and transmit with the same modulation at the same rate. The block diagram of the MC-CDMA transmitter is shown in Fig. 1. The input information sequence of the uth user is first converted into $N_c = 2K + 1$ parallel[1] data sequences $b^u_{-K,n}, \ldots, b^u_{0,n}, \ldots, b^u_{K,n}$, where n is the time index. The data $b^u_{k,n} \in C_\mathcal{M}$ are $\mathcal{M}$-PSK-modulated and differentially[2] encoded at a rate of $1/T_{\mathrm{MC}}$, where $T_{\mathrm{MC}} = N_c \times T$ is the symbol duration after serial/parallel (S/P) conversion, T is the symbol duration before S/P, and $C_\mathcal{M} = \{\ldots, e^{j2\pi m/\mathcal{M}}, \ldots\}$, where $m \in \{0, \ldots, \mathcal{M} - 1\}$. The resulting S/P converter output is then spread with a random spreading code $c^u(t)$ at a rate of $1/T_c$. The spreading factor, which is defined as the ratio

[1] We selected an odd number of subcarriers to have a central frequency, but the model can easily be rearranged to operate with an even number of subcarriers.

[2] We can also use pilot symbols for coherent modulation and detection [12], but that is beyond the scope of this paper.
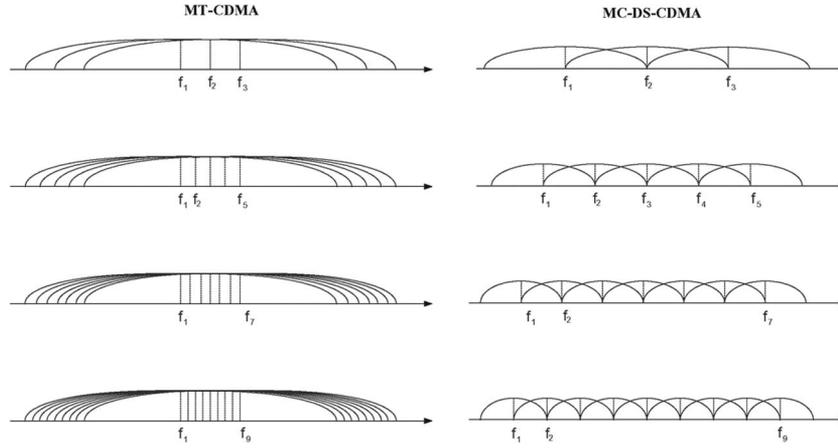
Fig. 2.   Different configurations of the MT-CDMA and MC-DS-CDMA within the same bandwidth.

between the chip and the symbol rates, is $L = T_{\mathrm{MC}}/T_c$. We write the spreading-code segment over the nth period T_{MC} as

$$c_n^u(t) = \sum_{l=0}^{L-1} c_{l,n}^u \phi(t - lT_c - nT_{\mathrm{MC}}) \tag{1}$$

where $c_{l,n}^u = \pm 1$ for $l = 0, \ldots, L-1$ is a random sequence of length L, and $\phi(t)$ is the chip pulse. We consider square-root-raised-cosine chip pulses with the roll-off factor β (see the Appendix). Closed-loop power control is taken into account at the transmitter by the amplification factor $a^u(t)$. All the data are then modulated in the baseband by the inverse discrete Fourier transform and summed to obtain the multicarrier signal. No guard interval is inserted. Indeed, the channel identification and equalization are achieved by the multicarrier spatiotemporal array receiver (MC-STAR) [13], and simulation results have shown that the guard-interval length does not affect the link-level performance. The MC-STAR exploits the intrinsic channel diversity by combining and equalizing the multipath signals. We, hence, eliminate the guard interval. Finally, the signal is transmitted after the radio-frequency upconversion.

The modulated subcarriers are orthogonal over the symbol duration T_{MC}. The frequency corresponding to the kth subcarrier is $f_k = \lambda \times k/T_{\mathrm{MC}}$. The transmitter belongs to the family of MT-CDMA if λ is set to one and to the class of MC-DS-CDMA if λ is set to L (see the resulting signal spectra in Fig. 2). Indeed, in an MT-CDMA system, the subcarrier frequencies are chosen to be orthogonal harmonics with the minimum frequency separation before spreading. By contrast, in the MC-DS-CDMA, the subcarrier frequencies are chosen to satisfy the orthogonality condition with the minimum possible frequency after spreading. The transmitted signal of the uth user is given by

$$s^u(t) = \sum_{k=-K}^{K} \sum_{n=-\infty}^{\infty} a^u(t) b_{k,n}^u c_n^u(t) e^{j2\pi f_k t}. \tag{2}$$

The transmitted bandwidth is

$$\mathrm{BW} = \frac{(N_c - 1)\lambda}{T_{\mathrm{MC}}} + \frac{(1+\beta)}{T_c}. \tag{3}$$

B. Channel Model

We consider an uplink transmission to M receiving antennas at the base station. The channel is assumed to be a slowly varying frequency-selective Rayleigh channel with a delay spread $\Delta\tau$. For each kth subcarrier of user u, the key channel parameter is the number of resolvable paths P_k^u, which is given by

$$P_k^u = \left\lfloor \frac{\Delta\tau}{T_c} \right\rfloor + 1 \tag{4}$$

where T_c is the chip duration. In practice, the number of multipaths depends also on the choice of the noise threshold used to differentiate between the received multipath components and the thermal noise. Typical delay-spread values are in the range of 0.4–4 μs in outdoor mobile radio channels, and the number of multipaths P_k^u varies between two and five with a 3.84-MHz resolution [15]. The M-dimensional complex low-pass equivalent vector representation of the impulse response experienced by subcarrier k of the uth user, for a receiver equipped with the M antennas, is

$$H_k^u(t) = \frac{\rho_k^u(t)}{(r^u)^e(t)} \sum_{p=1}^{P_k^u} \mathcal{G}_{k,p}^u(t) \delta\left(t - \tau_{k,p}^u(t)\right) \tag{5}$$

where $\rho_k^u(t)$ and $(r^u)^e(t)$ model the effects of shadowing and path loss, respectively, $r^u(t)$ is the distance from the uth user to the base station, and e is the path-loss exponent. We assume their variations in time to be very slow and, hence, nearly constant over several symbol durations. The M-dimensional complex vector $\mathcal{G}_{k,p}^u(t)^3$ denotes the fading and the array response from the user to the antenna elements of the receiver, and $\tau_{k,p}^u(t)$ represents the propagation time delay along the pth path. We note here that the large-scale path loss that includes free-space path loss and shadowing is the same for all the subcarriers of the same user. Moreover, the number of resolvable paths and their propagation time delays depend on the reflecting objects

---

[3] We may characterize $\mathcal{G}_{k,p}^u(t)$ in a space manifold that is parameterized by the angles of arrival [16]. However, a space characterization requires perfect antenna calibration and adequate sensor positioning.

and scatterers and can be assumed equal for all the subcarriers [17]. Therefore, we omit the index k from ρ, P, and τ ($\rho_k^u = \rho^u$, $P_k^u = P^u$, and $\tau_{k,p}^u = \tau_p^u$) and reformulate (5) as

$$H_k^u(t) = \frac{\rho^u(t)}{(r^u)^e(t)} \sum_{p=1}^{P^u} \mathcal{G}_{k,p}^u(t)\delta\left(t - \tau_p^u(t)\right). \quad (6)$$

A frequency-domain-channel model for a multicarrier system can be characterized by the coherence bandwidth[4] [17]

$$B_c \cong \frac{1}{2\pi\Delta\tau}. \quad (7)$$

When the frequency separation λ/T_{MC} is less than B_c, the MC-CDMA system is subject to correlated fading over different subcarriers. Fades across taps (multipaths) are mutually independent for the same carrier. However, fading for the same tap across different carriers is correlated. The envelope-correlation coefficient between subcarriers k and k' for user u is [17]

$$\rho_{k,k'}^u = E\left[\left|\mathcal{G}_{k,p,m}^u(t)\|\mathcal{G}_{k',p,m}^u(t+\tau)\right|\right]$$

$$= \frac{(1 + \lambda_{k,k'})\tilde{E}\left(\frac{2\sqrt{\lambda_{k,k'}}}{1+\lambda_{k,k'}}\right) - \frac{\pi}{2}}{2 - \frac{\pi}{2}} \quad (8)$$

with

$$\lambda_{k,k'} = \frac{J_0(2\pi f_D\tau)}{\sqrt{1 + \left[2\pi(f_k - f_{k'})\Delta\tau\right]^2}} \quad (9)$$

where E is the expectation function, $\mathcal{G}_{k,p,m}^u(t)$ is the fading and the antenna response from the user u to the antenna m of the receiver along the pth path, $\tilde{E}$ is the complete elliptic integral of the second kind, J_0 is the zeroth-order Bessel function, and f_D is the maximum Doppler frequency. We adopt the approach proposed in [18] and [19] to generate correlated Rayleigh channels across subcarriers. We also assume that the received channel multipath components across the M antennas are independent.

C. Received Signal

For a multicellular MC-CDMA system with C incell users and $N_c = 2K + 1$ carriers, the received signal is the superposition of signals from all users and all subcarriers. Hence, the M-dimensional observation vector received, after downconversion, by the antenna array can be expressed as follows:

$$X(t) = \sum_{u=1}^{C} \sum_{k=-K}^{K} \sum_{n=-\infty}^{\infty} H_k^u(t) \otimes a^u(t)b_{k,n}^u c_n^u(t)$$

$$\times e^{j2\pi(f_k+\Delta f^u)t} + N(t)$$

$$= \sum_{u=1}^{C} \sum_{k=-K}^{K} \sum_{n=-\infty}^{\infty} X_{k,n}^u(t) + N(t) \quad (10)$$

where $\otimes$ denotes time convolution, and Δf^u models the CFO, which is assumed to be equal for all the subcarriers. This is a realistic assumption since there is only one oscillator per transmitter (see Fig. 1). On the downlink, the CFO is even equal for all the incell users (i.e., $\Delta f^u = \Delta f \ \forall \ u \in \{1, \ldots, C\}$). The noise term $N(t)$ includes the thermal noise received at the antennas, as well as the outcell interference. The contribution $X_{k,n}^u(t)$ of the nth data symbol over the kth carrier of user u to the received vector $X(t)$ is given by

$$X_{k,n}^u(t) = H_k^u(t) \otimes a^u(t)b_{k,n}^u c_n^u(t)e^{j2\pi(f_k+\Delta f^u)t}$$

$$= \psi_k^u(t)b_{k,n} \sum_{p=1}^{Pu} G_{k,p}^u(t)\epsilon_{kp}^u(t)c_n^u\left(t - \tau_p^u\right)$$

$$\times e^{j2\pi(f_k+\Delta f^u)\left(t-\tau_p^u\right)}. \quad (11)$$

Along the pth path, $G_{k,p}^u(t) = (\sqrt{M}/\|\mathcal{G}_{k,p}^u(t)\|)\mathcal{G}_{k,p}^u(t)$ is the propagation vector over the kth subcarrier of the uth user with norm $\sqrt{M}$, and $(\epsilon_{k,p}^u)^2(t) = \|\mathcal{G}_{k,p}^u(t)\|^2/\sum_{p=1}^{P^u}\|\mathcal{G}_{k,p}^u(t)\|^2$ is the fraction of the total received power on the kth subcarrier of user u

$$(\psi_k^u)^2(t) = \left(\frac{\rho^u(t)}{(r^u)^e(t)}\right)^2 (a^u)^t(t)\sum_{p=1}^{Pu} \frac{\left\|\mathcal{G}_{k,p}^u(t)\right\|^2}{M}. \quad (12)$$

We define the matched–filtered observation vector of the frame number n over a time interval $[0, T_{MC})$ as

$$Y_n(t) = \frac{1}{T_c} \int_{D_\phi} X(nT_{MC} + t + t')\phi(t')dt' \quad (13)$$

where D_ϕ denotes the temporal support[5] of $\phi(t)$. After sampling at a multiple of the chip rate, we frame the observation into the overlapping blocks of constant length N_P. The oversampling ratio k_s is defined as the number of samples per chip. In the DS-CDMA and MT-CDMA systems, we need no more than one sample per chip ($k_s = 1$). In contrast, in the MC-DS-CDMA system, a higher sampling frequency is necessary for the receiver. Indeed, the sampling frequency has to satisfy the Nyquist sampling theorem, which states that the sampling interval must be smaller than the inverse of the double-sided bandwidth of the sampled signals. Hence, the smallest number greater than the number of subcarriers N_c is an adequate oversampling ratio for the MC-DS-CDMA. The resulting processing block duration $T_P = N_P(T_c/k_s)$ is equal to $T_{max} + \overline{\Delta\tau}$. The processing period $T_{max} = LT_c$ contains the N_c carrier symbols targeted for detection. The frame overlap $\overline{\Delta\tau} < T_{max}$, which is larger than the delay spread, allows multipath tracking [20]. Hence, we obtain the $M \times N_P$ matched–filtered observation matrix

$$\mathbf{Y}_n = [Y_n(0), Y_n(T_c/k_s), \ldots, Y_n((N_p-1)T_c/k_s)]. \quad (14)$$

---

[4]The coherence bandwidth is defined as the bandwidth over which the envelope correlation is above 0.5.

[5]For a rectangular pulse, D_ϕ is $[0, T_c]$. In practice and as assumed in this paper, it is the temporal support of a truncated square-root-raised cosine $D_\phi = [-N_{src}T_c, N_{src}T_c]$, where N_{src} stands for the truncation span of the shaping pulse in chip samples around zero.

It can be expressed as

$$\mathbf{Y}_n = \sum_{u=1}^{C} \sum_{k=-K}^{K} \sum_{n'=-\infty}^{\infty} \mathbf{Y}_{n',k,n}^{u} + \mathbf{N}_n \qquad (15)$$

where the baseband-preprocessed thermal noise and the outcell interference contribute the $\mathbf{N}_n$ and where the symbol n' of carrier k of user u contributes its observation matrix $\mathbf{Y}_{n',k,n}^{u}$ obtained by

$$\mathbf{Y}_{n',k,n}^{u} = \left[Y_{n',k,n}^{u}(0), \dots, Y_{n',k,n}^{u} \left((N_p - 1)T_c/k_s \right) \right] \quad (16)$$

$$Y_{n',k,n}^{u}(t) = \frac{1}{T_c} \int_{D_\phi} X_{k,n'}^{u}(nT_{MC} + t + t')\phi(t')dt'. \qquad (17)$$

As a result of the stationarity assumptions stated in Section II-B, $Y_{n',k,n}^{u}(t)$ can be developed into

$$Y_{n',k,n}^{u}(t) \simeq e^{j2\pi\Delta f^u nT_{MC}} \psi_k^u(nT_{MC}) b_{k,n'}^{u} \frac{1}{T_c}$$

$$\times \sum_{p=1}^{P} \int_{D_\phi} G_{k,p}^{u}(nT_{MC} + t + t')$$

$$\cdot \epsilon_{k,p}^{u}(nT_{MC} + t + t')$$

$$\times e^{j2\pi f_k \left(nT_{MC} + t + t' - \tau_p^u \right)}$$

$$\times c_{n'}^{u} \left(nT_{MC} + t + t' - \tau_p^u \right) \phi(t')dt'$$

$$\simeq e^{j2\pi\Delta f^u nT_{MC}} \psi_k^u(nT_{MC}) b_{k,n'}^{u} V_{n',k,n}^{u}(t)$$

$$\simeq \psi_k^u(nT_{MC}) b_{k,n'}^{u} U_{n',k,n}^{u}(t) \qquad (18)$$

where the spread channel vector without the CFO $V_{n',k,n}^{u}(t)$ is obtained by

$$V_{n',k,n}^{u}(t) = \frac{1}{T_c} \int_{D_\phi} H_k^u(nT_{MC} + t + t') \otimes c_{n'}^{u}(nT_{MC} + t + t')$$

$$\cdot e^{j2\pi f_k(nT_{MC} + t + t')} \phi(t')dt' \qquad (19)$$

and the spread channel vector is

$$U_{n',k,n}^{u}(t) = e^{j2\pi\Delta f^u nT_{MC}} V_{n',k,n}^{u}(t). \qquad (20)$$

We assumed in the development of (18) that $\psi_k(nT_G + t + t')$ is constant during the interval $t' \in D_\phi$. We also considered that the frequency offset is small compared to the symbol rate $(\Delta f^u T_{MC} \ll 1)$; thus; $e^{j2\pi\Delta f^u(nT_{MC} + t + t')} \simeq e^{j2\pi\Delta f^u nT_{MC}}$ for $t' \in D_\phi$ and $t \in [0, T_{MC})$. Replacing (18) into (15) gives

$$\mathbf{Y}_n = \sum_{u=1}^{C} \sum_{k=-K}^{K} \sum_{n'=-\infty}^{\infty} b_{k,n'}^{u} \psi_{k,n}^{u} e^{j2\pi\Delta f^u nT_{MC}} \mathbf{V}_{n',k,n}^{u} + \mathbf{N}_n$$

$$= \sum_{u=1}^{C} \sum_{k=-K}^{K} \sum_{n'=-\infty}^{\infty} b_{k,n'}^{u} \psi_{k,n}^{u} \mathbf{U}_{n',k,n}^{u} + \mathbf{N}_n \qquad (21)$$

where $\psi_{k,n}^{u} = \psi_k^u(nT_{MC})$. Due to asynchronism and multipath propagation, each user's carrier observation matrix carries the information from the current and as well as from the previous and future symbols of the corresponding user's carrier. We therefore have

$$\mathbf{Y}_n = \sum_{u=1}^{C} \sum_{k=-K}^{K} \sum_{n'=n-1}^{n+1} b_{k,n'}^{u} \psi_{k,n}^{u} \mathbf{U}_{n',k,n}^{u} + \mathbf{N}_n. \qquad (22)$$

D. Interference Analysis

Without loss of generality, let us focus on the detection of the nth symbol carried by the kth carrier of the desired user-assigned index $d \in \{1, \dots, C\}$, i.e., b_{k^d,n^d}^{d}. Using (22) and defining a vector $\underline{V}$ as a matrix $\mathbf{V}$ reshaped columnwise, we can rewrite the observation matrix for a desired user d with respect to its nth symbol of carrier k targeted for detection in the following simpler vector form:

$$\underline{Y}_n = \underbrace{s_{k,n}^{d} \underline{U}_{n,k,n}^{d}}_{\text{desired signal}} + \underbrace{\sum_{\substack{u=1 \\ u \neq d}}^{C} \sum_{k'=-K}^{K} \sum_{n'=n-1}^{n+1} s_{k',n'}^{u} \underline{U}_{n',k',n}^{u}}_{\underline{I}_{\text{MAI},k,n}^{d}}$$

$$+ \underbrace{\sum_{\substack{k'=-K \\ k' \neq k}}^{K} \sum_{n'=n-1}^{n+1} s_{k',n'}^{d} \underline{U}_{n',k',n}^{d}}_{\underline{I}_{\text{ICI},k,n}^{d}} + \underbrace{\sum_{\substack{n'=n-1 \\ n' \neq n}}^{n+1} s_{k,n'}^{d} \underline{U}_{n',k,n}^{d}}_{\underline{I}_{\text{ISI},k,n}^{d}} + \underline{N}_n$$

$$= s_{k,n}^{d} \underline{U}_{n,k,n}^{d} + \underline{I}_{k,n}^{d} + \underline{N}_n \qquad (23)$$

where $s_{k',n'}^{u} = \psi_{k',n}^{u} b_{k',n'}^{u}$ and $(\psi_{k,n}^{u})^2$ are the n'th signal component of the k'th carrier of user u and the received power of user u over carrier k, respectively. The total interference $\underline{I}_{k,n}^{d}$ includes the following three types of interference: 1) The MAI $\underline{I}_{\text{MAI},k,n}^{d}$ is the interference due to the N_c carriers from the other incell users $u \neq d$. 2) The ICI $\underline{I}_{\text{ICI},k,n}^{d}$ is the interference due to the other carriers $k' \neq k$ from the same user d. 3) The ISI $\underline{I}_{\text{ISI},k,n}^{d}$ is the interference due to the same carrier k from the same user d. The noise vector $\underline{N}_n$, which comprises the preprocessed thermal noise and the interference due to the out-of-cell users, is assumed to be uncorrelated both in space and time with variance σ_n^2.

In previous work [13], we have assumed the interference $\underline{I}_{k,n}^{d}$ to be an another contribution to the noise $\underline{N}_n$. Hence, the signal component of the desired user's carrier is extracted by the spatiotemporal MRC as follows:

$$\widehat{s}_{k,n}^{d} = \underline{W}_{\text{MRC},k,n}^{d^H} \underline{Y}_n = \frac{\widehat{\underline{U}}_{n,k,n}^{d^H} \underline{Y}_n}{\left\| \widehat{\underline{U}}_{n,k,n}^{d} \right\|^2} \qquad (24)$$

where, anywhere in the paper, the notation $\widehat{\alpha}$ stands for an estimate of a given variable α, $(\cdot)^H$ is the Hermitian operator, and $\underline{W}_{\text{MRC},k,n}^{d}$ is the MRC beamformer. Equation (23) shows that the net interference increases with the number of interferers and subcarriers, which severely limits the capacity of the

MC-CDMA system with simple MRC receivers. Therefore, in the next section, we shall use the data decomposition of (23) to formulate the interference-suppression problem and propose a new MC-CDMA receiver with full-interference-suppression capabilities.

III. PROPOSED MC-CDMA RECEIVER

This section is dedicated to the description, the performance analysis, and the implementation of the proposed MC-ISR receiver.

A. Multicarrier Interference Subspace Rejection (MC-ISR)

Provided that an estimate of the total interference $\widehat{\underline{I}}_{k,n}^d = \widehat{\underline{I}}_{\mathrm{MAI},k,n}^d + \widehat{\underline{I}}_{\mathrm{ICI},k,n}^d + \widehat{\underline{I}}_{\mathrm{ISI},k,n}^d$ is made available at the receiver (see Section III-C), we can eliminate it and still achieve a distortionless response to the desired signal by imposing the following simple constraints to the combiner $\underline{W}_{k,n}^d$:

$$\begin{cases} \underline{W}_{k,n}^{d\mathrm{H}} \widehat{\underline{U}}_{n,k,n}^d = 1 \\ \underline{W}_{k,n}^{d\mathrm{H}} \widehat{\underline{I}}_{k,n}^d = 0 \end{cases}$$

$$\rightarrow \begin{cases} \underline{W}_{k,n}^{d\mathrm{H}} \widehat{\underline{U}}_{n,k,n}^d = 1 \\ \underline{W}_{k,n}^{d\mathrm{H}} \left(\widehat{\underline{I}}_{\mathrm{MAI},k,n}^d + \widehat{\underline{I}}_{\mathrm{ICI},k,n}^d \widehat{\underline{I}}_{\mathrm{ISI},k,n}^d \right) = 0. \end{cases} \quad (25)$$

The first constraint guarantees a distortionless response to the desired signal, whereas the second one directs a null to the total interference realization and, thereby, cancels it. Exploiting the general framework developed in [11], the solution to the specific optimization problem in (25) is the MC-ISR combiner $\underline{W}_{k,n}^d$ that is given as follows:

$$Q_n = 1/\left(\widehat{\underline{I}}_{k,n}^{d\mathrm{H}} \widehat{\underline{I}}_{k,n}^d \right) = 1/\left\| \widehat{\underline{I}}_{k,n}^d \right\|^2 \quad (26)$$

$$\mathbf{II}_{k,n}^d = \mathbf{I}_{N_T} - \widehat{\underline{I}}_{k,n}^d \widehat{\underline{I}}_{k,n}^{d\mathrm{H}} \times Q_n \quad (27)$$

$$\underline{W}_{k,n}^d = \frac{\mathbf{II}_{k,n}^d \widehat{\underline{U}}_{n,k,n}^d}{\widehat{\underline{U}}_{n,k,n}^{d\mathrm{H}} \mathbf{II}_{k,n}^d \widehat{\underline{U}}_{n,k,n}^d} \quad (28)$$

where $N_T = M \times N_P$ is the total space dimension, and $\mathbf{I}_{N_T}$ denotes an $N_T \times N_T$ identity matrix. First, we form the projector $\mathbf{II}_{k,n}^d$ orthogonal to the total interference realization. Second, we project the estimated response vector $\widehat{\underline{U}}_{n,k,n}^d$ and normalize it to derive the combiner. We use this combiner instead of the MRC to extract the nth signal component of the kth carrier of the desired user as

$$\widehat{s}_{k,n}^d = \underline{W}_{k,n}^{d\mathrm{H}} \underline{Y}_n. \quad (29)$$

Unlike most of the multiuser receivers proposed for the MC-CDMA, which focus on the MAI while ignoring the ICI,

the MC-ISR fully suppresses the total interference resulting from the MAI, the ISI, and the ICI by simple yet efficient nulling.[6] Simulation results will later show that the ICI is not negligible and that full interference suppression is required to improve MC-CDMA-system performance.

B. Link-/System-Level Performance Analysis

This section is dedicated to the performance analysis of the MC-ISR receiver based on the GA. We exploit the analysis results of the DS-CDMA ISR recently developed in [21] at the link level and extend them to the MC-ISR. Additionally, we broaden the scope of the analysis to the system level.

1) Link-Level Performance: For the sake of simplicity, we assume temporarily perfect channel identification and perfect CFO estimation and recovery. Later, in the simulations, we will use the channel and the CFO estimates provided by the MC-STAR[7] [13]. The postcombined signal can be formulated as

$$\widehat{s}_{k,n}^d = \underline{W}_{k,n}^{d^H} \underline{Y}_n$$

$$= s_{k,n}^d \delta_{\mathrm{MAI},k,n}^d \delta_{\mathrm{ICI},k,n}^d + \delta_{\mathrm{ISI},k,n}^d \underline{W}_{k,n}^{d^H} \underline{N}_n \quad (30)$$

where $\delta_{\mathrm{MAI},k,n}^d$, $\delta_{\mathrm{ICI},k,n}^d$, and $\delta_{\mathrm{ISI},k,n}^d$ are the combining residuals of $\underline{I}_{\mathrm{MAI},k,n}^d$, $\underline{I}_{\mathrm{ICI},k,n}^d$, and $\underline{I}_{\mathrm{ISI},k,n}^d$, respectively. We assume here that the interference-rejection residuals $\delta_{\mathrm{MAI},k,n}^d$, $\delta_{\mathrm{ICI},k,n}^d$, and $\delta_{\mathrm{ISI},k,n}^d$ are the Gaussian random variables with a zero mean. Hence, we only need to evaluate their variances. Note that the residuals would be null (i.e., $\delta_{\mathrm{MAI},k,n}^d = \delta_{\mathrm{ICI},k,n}^d = \delta_{\mathrm{ISI},k,n}^d = 0$) if the reconstruction of the interference were perfect (i.e., $\widehat{\underline{I}}_{k,n}^d = \underline{I}_{k,n}^d$), and hence, $\widehat{s}_{k,n}^d = s_{k,n}^d + \underline{W}_{k,n}^{d^H} \underline{N}_n$ would be corrupted only by the residual noise, which is Gaussian with a zero mean and a variance

$$\mathrm{Var}\left[\underline{W}_{k,n}^{d^H} \underline{N}_n \right] = \overline{\kappa} \sigma_N^2 \quad (31)$$

where $\overline{\kappa} = E[\|\underline{W}_{k,n}^d\|^2] = (ML-1)/(ML-2)$ is a measure of the enhancement of the white noise compared to the MRC ($\overline{\kappa} = 1$ for the MRC) [21]. However, in practice, the interference vector is erroneously reconstructed due to wrong tentative data decisions and power-control errors, and hence, $\widehat{s}_{k,n}^d$ is further corrupted by nonnull residual interference-rejection components. Therefore, we introduce the error-indicating variables $\xi_{k,n}^u = \widehat{b}_{k,n}^{u*} b_{k,n}^u$ and $\lambda_{k,n}^u = \widehat{\psi}_{k,n}^{u*} \psi_{k,n}^u / \|\widehat{\psi}_{k,n}^u\|^2$, where $(\cdot)^*$ means complex conjugate. $\xi_{k,n}^u$ models the symbol-estimation error provided by the MRC at the initial stage. $\lambda_{k,n}^u$ characterizes the power-control error. $\xi_{k,n}^u$ and $\lambda_{k,n}^u$ are equal to one when the estimated data symbol and the

---

[6]The formulation of the MC-ISR can be extended to the MMSE-type criteria [11].

[7]Simulations will show a little deviation from the analysis in the operating BER region.

power control are perfect; otherwise, they are complex numbers. Since $\underline{Y}^u_{n',k',n} = s^u_{k',n'}\underline{U}^u_{n',k',n} = b^u_{k',n'}\psi^u_{k',n}\underline{U}^u_{n',k',n} = \xi^u_{k',n'}\lambda^u_{k',n}\widehat{b}^u_{k',n'}\widehat{\psi}^u_{k',n}\underline{U}^u_{n',k',n} = \xi^u_{k',n'}\lambda^u_{k',n}\underline{\widehat{Y}}^u_{n',k',n}$,[8]

we can rewrite (23) as

$$
\underline{Y}_n = \underline{Y}^d_{n,k,n} + \sum_{\substack{u=1 \\ u \neq d}}^{C} \sum_{k'=-K}^{K} \sum_{n'=n-1}^{n+1} \xi^u_{k',n'}\lambda^u_{k',n}\underline{\widehat{Y}}^u_{n',k',n}
$$

$$
+ \sum_{\substack{k'=-K \\ k' \neq k}}^{K} \sum_{n'=n-1}^{n+1} \xi^d_{k',n'}\lambda^d_{k',n}\underline{\widehat{Y}}^d_{n',k',n}
$$

$$
+ \sum_{\substack{n'=n-1 \\ n' \neq n}}^{n+1} \xi^d_{k,n'}\lambda^d_{k,n}\underline{\widehat{Y}}^d_{n',k,n} + \underline{N}_n. \tag{32}
$$

The signal after the MC-ISR combining is then

$$
\underline{W}^{d\mathrm{H}}_{k,n}\underline{Y}_n
$$

$$
= s^d_{k,n} + \sum_{\substack{u=1 \\ u \neq d}}^{C} \sum_{k'=-K}^{K} \sum_{n'=n-1}^{n+1} \xi^u_{k',n'}\lambda^u_{k',n}\underline{W}^{d\mathrm{H}}_{k,n}\underline{\widehat{Y}}^u_{n',k',n}
$$

$$
+ \sum_{\substack{k'=-K \\ k' \neq k}}^{K} \sum_{n'=n-1}^{n+1} \xi^d_{k',n'}\lambda^d_{k',n}\underline{W}^{d\mathrm{H}}_{k,n}\underline{\widehat{Y}}^d_{n',k',n}
$$

$$
+ \sum_{\substack{n'=n-1 \\ n' \neq n}}^{n+1} \xi^d_{k,n'}\lambda^d_{k,n}\underline{W}^{d\mathrm{H}}_{k,n}\underline{\widehat{Y}}^d_{n',k,n} + \underline{W}^{d\mathrm{H}}_{k,n}\underline{N}_n. \tag{33}
$$

The MC-ISR combiner $\underline{W}^d_{k,n}$ satisfies the optimization property in (25), and thus

$$
\underline{W}^{d\mathrm{H}}_{k,n}\underline{\widehat{I}}^d_{k,n} = 0 \Longrightarrow \mathrm{Var}\left[\underline{W}^{d\mathrm{H}}_{k,n}\left(\underline{\widehat{I}}^d_{\mathrm{MAI},k,n}\right.\right.
$$

$$
\left.\left. + \underline{\widehat{I}}^d_{\mathrm{ICI},k,n} + \underline{\widehat{I}}^d_{\mathrm{ISI},k,n}\right)\right] = 0. \tag{34}
$$

---

[8]Here, we assume a perfect time and frequency synchronization.

This result allows the derivation of the variance of the interference-rejection residuals, as shown in the Appendix. Let $\overline{\psi}^2_D = E[(\psi^d_k)^2]$ be the average power of the kth carrier of the desired user and $\overline{\psi}^2_I$ be the average interference power on each interfering carrier. The variances of the residual $\underline{I}^d_{\mathrm{MAI},k,n}$ can be written as

$$
\mathrm{Var}\left[\delta^d_{\mathrm{MAI},k,n}\right] = (C-1)\frac{\overline{\psi}^2_I}{L}\left[\varsigma(\beta) + \chi_k(\beta)\right](1 + \rho_\lambda - \rho_\xi)\overline{\kappa} \tag{35}
$$

where $\varsigma(\beta) = 1 - (\beta/4)$

$$
\chi_k(\beta) = \begin{cases} \frac{\beta}{8}, & \text{if } k = -K \text{ or } K \\ \frac{\beta}{4}, & \text{if } k = -K+1, \ldots, K-1 \end{cases} \tag{36}
$$

for the MC-DS-CDMA ($\lambda = L$ and $f_k = k/T_\mathrm{c}$), and

$$
\chi_k(\beta) = \sum_{\substack{k'=-K \\ k' \neq k}}^{K} \vartheta\left(|k-k'|\right) \tag{37}
$$

where $\vartheta(x)$ is defined in (38), shown at the bottom of the page, for the MT-CDMA ($\lambda = 1$ and $f_k = k/T_\mathrm{MC}$). The expressions of $\rho_\xi = E[\xi^u_{k',n'}\lambda^u_{k',n}\xi^{u\,*}_{k',n'}\lambda^{u\,*}_{k',n}]$ and $\rho_\lambda = E[(\lambda^u_{k,n})^2] - 1$ are derived for a Rayleigh fading channel with P paths to yield

$$
\rho_\xi = \left(1 - (1 - \cos(2\pi/\mathcal{M}))S_\mathrm{rec}\right)^2
$$

$$
\rho_\lambda = \frac{4\pi^2(f_\mathrm{D} \times \tau_\mathrm{PC})^2}{P-1} \tag{39}
$$

where S_rec is the symbol-error rate in the previous MC-ISR stage, f_D is the maximum Doppler frequency, and τ_PC is the power-control feedback delay. The variances of the residuals $\underline{I}^d_{\mathrm{ICI},k,n}$ and $\underline{I}^d_{\mathrm{ISI},k,n}$ can be written as

$$
\mathrm{Var}\left[\delta^d_{\mathrm{ICI},k,n}\right] = \frac{\overline{\psi}^2_D}{L}\delta_\mathrm{is}\chi_k(\beta)(1 + \rho_\lambda - \rho_\xi)\overline{\kappa}
$$

$$
\mathrm{Var}\left[\delta^d_{\mathrm{ISI},k,n}\right] = \frac{\overline{\psi}^2_D}{L}\delta_\mathrm{is}\varsigma(\beta)(1 + \rho_\lambda - \rho_\xi)\overline{\kappa} \tag{40}
$$

where $\delta_\mathrm{is} = (P-1)/P$ is a measure of the relative impact of the interference generated by the other paths on a given path of the desired user (for a Rayleigh fading channel with P

$$
\vartheta(x) = \begin{cases} 1 - \frac{\beta}{2} - \frac{x}{2L} + \frac{3\beta}{4\pi}\sin\left(\frac{\pi x}{\beta L}\right) + \left(\frac{\beta}{4} - \frac{x}{4L}\right)\cos\left(\frac{\pi x}{\beta L}\right), & \text{if } 0 \leq x/L \leq \min(\beta, 1-\beta) \\[2mm] 1 - \frac{x}{L}, & \text{if } \beta \leq x/L \leq 1-\beta \text{ and } \beta < 0.5 \\[2mm] \frac{3}{4} - \frac{\beta}{4} - \frac{x}{4L} + \frac{3\beta}{4\pi}\sin\left(\frac{\pi x}{\beta L}\right) + \left(\frac{\beta}{4} - \frac{x}{4L}\right)\cos\left(\frac{\pi x}{\beta L}\right) + \frac{3\beta}{8\pi}\sin\left(\frac{\pi x}{\beta L} - \frac{\pi}{\beta}\right) \\ \quad - \left(\frac{x}{8L} - \frac{1-\beta}{8}\right)\cos\left(\frac{\pi x}{\beta L} - \frac{\pi}{\beta}\right), & \text{if } 1-\beta \leq x/L \leq \beta \text{ and } \beta > 0.5 \\[2mm] \frac{3}{4} + \frac{\beta}{4} - \frac{3x}{4L} + \frac{3\beta}{8L}\sin\left(\frac{\pi x}{\beta L} - \frac{\pi}{\beta}\right) - \left(\frac{x}{8L} - \frac{1-\beta}{8}\right)\cos\left(\frac{\pi x}{\beta L} - \frac{\pi}{\beta}\right), & \text{if } \max(\beta, 1-\beta) \leq x/L \leq 1 \end{cases} \tag{38}
$$

equal paths). The signal-to-interference-plus-noise ratio (SINR) on the kth carrier can be estimated using (41), shown at the bottom of the page. Note that the SINR expression above also applies to the MRC by setting $\overline{\kappa} = 1$ and $\rho_\lambda = \rho_\xi = 0$ in (35) and (40). Note also that in [22], we provide the variance of the interference for an MC-CDMA system with a rectangular pulse. In this paper, we improve the analytical analysis by deriving the variance of the interference with a more practical band-limited square-root-raised-cosine waveform. The bit-error-rate (BER) performance on the kth carrier is then given as follows:

$$P_e^k = \Omega(\text{SINR}_{\text{ISR},k}) \tag{42}$$

where Ω represents the single-user bound (SUB), which is classically defined as a conditional Gaussian Q-function over ψ_D and ψ_I. When using this classical representation, the average BER is derived by first finding the probability density functions (pdfs) of ψ_D and ψ_I and then by averaging over those pdfs. Since it is difficult to find a simple expression for the pdfs of ψ_D and ψ_I, which takes into consideration antenna diversity, imperfect power control, and imperfect channel identification, we may consider an approximative pdf. In this analysis, we choose to simulate Ω without imposing any pdf approximation. For each multicarrier configuration, we run single-user and single-carrier link-level simulations. We reproduced as much as possible most of the real-world operating conditions: time and frequency synchronization, imperfect power control, channel-identification errors, antenna diversity, etc. These link-level simulations gave a realistic $\Omega : \text{BER} = \Omega(\text{SNR})$. The simulations will later consider a multiuser and multicarrier environment. The average BER performance of the MC-ISR receiver is given by

$$P_e = \frac{1}{2K+1} \sum_{k=-K}^{K} P_e^k. \tag{43}$$

2) System-Level Performance: In order to compare the different MC-ISR configurations, the link-level curves provide a good picture of the performance of each system. However, limiting comparisons to the BER performance is not sufficient because the data rate is not equal for all configurations. Hence, we translate the link-level results into the system-level results in terms of the total throughput under the following three assumptions: 1) All users are received with an equal average power (i.e., $\overline{\psi}_D^2 = \overline{\psi}_I^2$) [1]. 2) All the cells have the same average load of C users per cell. 3) The outcell-to-incell interference ratio f is set to 0.6 [23]. Given these assumptions in an interference-limited system (the thermal noise is low compared to the

interference), the link-level SIR at the base-station antennas (ignoring the ISI for simplicity) is

$$\text{SIR}_{\text{ISR}} = \frac{1}{(C-1)\alpha + \frac{1}{L}\delta_{\text{is}}\chi(\beta)(1+\rho_\lambda-\rho_\xi)\overline{\kappa} + Cf\gamma} \tag{44}$$

where

$$\chi(\beta) = \max_k[\chi_k(\beta)]$$

$$\alpha = \frac{1}{L}\left(\varsigma(\beta) + \chi(\beta)\right)(1+\rho_\lambda-\rho_\xi)\overline{\kappa}$$

$$\gamma = \frac{1}{L}\left(\varsigma(\beta) + \chi(\beta)\right)\overline{\kappa}. \tag{45}$$

$(C-1)\alpha$ is the normalized variance of the residual MAI $(u \neq d)$, $(1/L)\delta_{\text{is}}\chi(\beta)(1+\rho_\lambda-\rho_\xi)\overline{\kappa}$ is the normalized variance of the residual ICI $(k' \neq k$ and $u = d)$, and $Cf\gamma$ is the normalized variance of the outcell interference. Note that we assumed in the development of (44), which is derived from (41), negligible thermal noise and ISI.

The maximum number of users that can access the system $C_{\max}$ can, hence, be calculated by the simple procedure illustrated in Table I. After initialization, this procedure increments the capacity C until the SIR_{ISR} given by (44) no longer exceeds the required SNR_{req}. The SNR_{req} is the required SNR, derived from link-level simulations, to meet a BER of 5% in order to achieve a QoS of 10^{-6} after channel decoding. In step 2.2, we use the fact that the SIR expression applies to the MRC by setting $\overline{\kappa} = 1$ and $\rho_\lambda = \rho_\xi = 0$ in (44). In step 2.3, we evaluate the symbol-error rate S_{MRC} after the MRC stage as follows:

$$S_{\text{MRC}} = \Omega(\text{SIR}_{\text{MRC}}) \tag{46}$$

where Ω represents the SUB. Note that the multistage MC-ISR is considered in step 2.5. The total throughput is, hence, $\mathcal{T}_{\max} = C_{\max} \times R_{\text{b}} = C_{\max} \times R_{\text{s}} \times \log_2(\mathcal{M})$, where R_{b} and R_{s} are the bit rate and the symbol rate over all subcarriers, respectively.

C. MC-ISR Receiver Implementation

As mentioned in Section III-A, the proposed MC-ISR receiver requires accurate channel-parameter estimates and data decisions to reconstruct the total interference $\widehat{I}_{k,n}^d$ and to reliably null it. Unlike the previous works on interference suppression or multiuser detection [3], [6], which assume perfect knowledge of the channel, we propose here a full space–time-receiver solution that jointly implements channel identification and synchronization both in time and frequency using the MC-STAR [13], as well as the signal combining

$$\text{SINR}_{\text{ISR},k} = \frac{\overline{\psi}_D^2}{\text{Var}\left[\delta_{\text{MAI},k,n}^d\right] + \text{Var}\left[\delta_{\text{ICI},k,n}^d\right] + \text{Var}\left[\delta_{\text{ISI},k,n}^d\right] + \overline{\kappa}\sigma_N^2} \tag{41}$$

TABLE I
CAPACITY COMPUTATION PROCEDURE

```
1. Initialize capacity C = 0
2. Start computation loop:
2.1 Increment capacity C = C + 1
2.2 Compute the SIR with MRC
        SIR_MRC = L / ((C-1)(ς(β)+χ(β))+χ(β)δ_is+fC(ς(β)+χ(β)))
2.3 Compute the symbol error rate SER after MRC stage
        S_MRC = Ω(SIR_MRC)
2.4 Compute ρ_λ and ρ_ξ
2.5 Compute the SIR
        SIR_ISR_1 = 1 / ((C-1)α+ (1/L) δ_is χ(β)(1+ρ_λ-ρ_ξ)κ̄+Cfγ)
        If number of stages S > 1 start the loop, else goto 2.6
          For s = 2 : S
          Compute the symbol error rate SER after the s − 1 stage
                S_ISR_{s-1} = Ω(SIR_ISR_{s-1})
          Compute ρ_ξ
          Compute the SIR
                SIR_ISR_s = 1 / ((C-1)α+ (1/L) δ_is χ(β)(1+ρ_λ-ρ_ξ)κ̄+Cfγ)
          End
2.6 if SIR_ISR_s > SNR_req goto 2.1, else exit
3. Decrement capacity C = C − 1
```

with full-interference-suppression capabilities. Fig. 1 shows the block diagram of the proposed receiver implementation, which is divided in four main modules. The first module is a preprocessor that downconverts the received signal to the baseband and then passes it through the chip-matched filter before sampling and data-block framing. The second module is a signal combiner that provides symbol estimates from the data observation, first by the MRC in an initial iteration and then by the MC-ISR in one or more iterative stages. The third module is a channel identifier and synchronizer from the MC-STAR that implements closed-loop CFOR and estimates all the channel parameters (multipath time delays and their phases and amplitudes, received power, and CFO). The fourth module is a null-constraint generator common to all incell users. It gathers the data decisions and channel-parameter estimates from the second and third modules dedicated to each incell user/carrier pair in order to reconstruct the total incell signal vector $\underline{I}_n$. Then, to each combiner, say, of the desired user/carrier pair as shown in Fig. 1, it passes on the associated null constraint (i.e., $\underline{I}_{k,n}^d = \underline{I}_n - s_{k,n}^d \underline{U}_{n,k,n}^d$) calculated with the least computations by simple subtraction from $\underline{I}_n$ of the desired-signal contribution from the corresponding user/carrier pair.

The implementation of the closed-loop CFOR[9] jointly with the multicarrier and multiuser detection (here by the MC-ISR) requires careful attention regarding the order in which these two tasks should be processed. Indeed, the conventional operation of the CFOR at an early processing stage[10] prior to interference suppression would require (on the uplink only) as many independently CFO-compensated observations and interference null constraints as received incell users, thereby resulting in a tremendous complexity increase. Here, we develop an efficient postinterference-suppression CFOR scheme by splitting the MC-ISR-combining operation of (29) into two steps—an

observation-cleaning projection and an MRC combining—and by inserting CFO compensation in between as follows:

$$\underline{Y}_{\Pi,k,n}^d = \mathbf{\Pi}_{k,n}^d \underline{Y}_n \tag{47}$$

$$\widehat{\Delta f}_n^d = \widehat{\Delta f}_{n-1}^d + \widehat{\delta f}_n^d \tag{48}$$

$$\dot{\underline{Y}}_{\Pi,k,n}^d = \underline{Y}_{\Pi,k,n}^d e^{-j2\pi \widehat{\Delta f}_n^d nT} \tag{49}$$

$$\widehat{\underline{V}}_{\Pi,k,n}^d = \mathbf{\Pi}_{k,n}^d \widehat{\underline{V}}_{k,n}^d \tag{50}$$

$$\widehat{s}_{k,n}^d = \frac{\widehat{\underline{V}}_{\Pi,k,n}^{d\mathrm{H}} \dot{\underline{Y}}_{\Pi,k,n}^d}{\left\| \widehat{\underline{V}}_{\Pi,k,n}^d \right\|^2}. \tag{51}$$

The cleaning projection of (47) results in an "almost interference-free" observation $\underline{Y}_{\Pi,k,n}^d$ and allows for CFO estimation and compensation in (48) and (49), respectively, using the CFOR module of the single-user MC-STAR [see to [13] and [24] for the details on how to estimate the CFO adjustment term in (49)] and for MRC combining in (51) using the projected estimate of the spread channel vector without the CFO $\widehat{\underline{V}}_{\Pi,k,n}^d$. To the best of our knowledge, we are the first to report on and address this issue and to propose an efficient scheme for closed-loop CFOR in a multiuser-detection context. It is important to mention here that if $\Delta f^u = \Delta f \ \forall u \in \{1,\ldots,C\}$ (i.e., downlink), then there is no need to estimate the CFO for the MC-ISR to null the incell interference. Indeed, the MC-ISR combiner $\underline{W}_{k,n}^d$ satisfies the optimization property in (25). Thus, it is not affected by the CFO of other users, i.e.,

$$\underline{W}_{k,n}^{d\mathrm{H}} \widehat{\underline{I}}_{k,n}^d = 0 \implies e^{j2\pi\Delta f nT_{\mathrm{MC}}} \left[\underline{W}_{k,n}^{d\mathrm{H}} \widehat{\underline{I}}_{k,n}^d \right] = 0. \tag{52}$$

Once the MC-ISR projection is performed in (47) after the reconstruction of $\widehat{\underline{I}}_{k,n}^d$ without the CFO, we implement the same CFOR scheme implemented in part by (48) and (49). Hence, like the near–far resistant detector proposed in [10], the multiuser CFOR problem can be transformed on the downlink into a single-user CFOR problem, and conventional single-user methods can therefore be used to estimate the frequency offset.[11]

To validate the efficiency of the proposed CFOR strategy in a multicarrier- and multiuser-detection scheme on the uplink, we consider a multiuser DBPSK MT-CDMA system with seven subcarriers, a spreading factor of 96, and five incell users ($N_c = 7$, $L = 96$, and $C = 5$). We select the setup that will be introduced in Section IV-A. The frequency offset normalized by the subcarrier separation ($\Delta f \times T_{\mathrm{MC}}$) is set to 0.005 (i.e., $\Delta f = 200$ Hz).[12] Fig. 3 shows the link-level results of the MC-ISR with and without a CFOR. Results suggest that a CFO of 200 Hz has a serious impact on the performance of the MC-CDMA and that the link-level gain with the proposed CFOR is in the range of 1 dB at a BER of 5% before channel

---

[9]In contrast to the open-loop structures, the closed-loop CFOR reduces the channel time variations and greatly improves their tracking [13].

[10]Usually, the CFOR is embedded in the RF chain or plugged to preprocessor output.

[11]The study of the CFOR performance is provided in [13].

[12]We select $\Delta f = 200$ Hz to show that even CFO residuals below the maximum value tolerated by the 3G standards result in significant losses in performance.
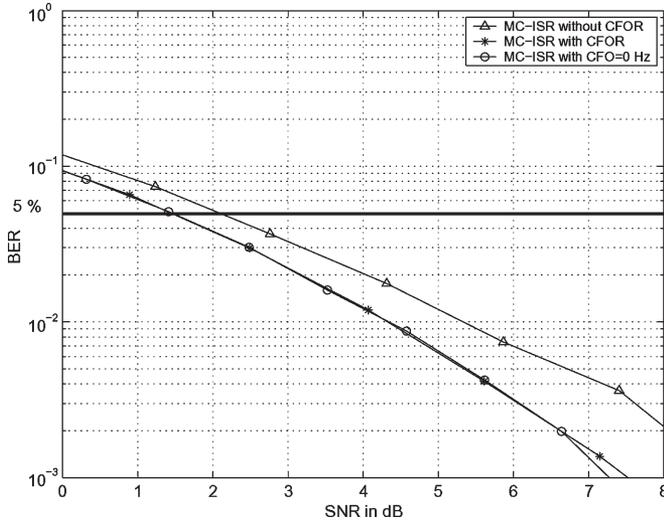
Fig. 3.   BER versus SNR for the MT-CDMA MC-ISR, $L = 96$, $N_c = 7$, and $C = 5$, with and without CFOR.

Parameter	Value	Comment
BW_{max}	5 MHz	maximum bandwidth
M	2	number of antennas
f_c	1.9 GHz	central carrier frequency
f_D	8.8 Hz	Doppler frequency (5 kmph)
Δf	200 Hz	frequency offset
f_{PC}	1600 Hz	frequency of PC updating
Δ_{PC}	± 0.25 dB	power control adjustment
PC^{max}_{min}	± 30 dB	power control range
BER_{PC}	5%	simulated PC bit error rate
$\frac{\delta \tau}{\delta t}$	0.049 ppm	time-delay drift
$\Delta \tau$	4 chips	delay spread
L_g	0	guard interval length
N_s	2	number of multistages
β	0.22	rolloff factor
$2N_{src} + 1$	9	number of pulse samples

decoding. By comparing the link-level curves of the MC-ISR with a CFOR and the MC-ISR without a frequency offset (i.e., CFO = 0 Hz), we notice that the CFOR almost completely compensates the performance loss due to the frequency offset. These results confirm the need for and the efficiency of the proposed CFOR in a multicarrier- and multiuser-detection context.

IV. SIMULATION RESULTS

A. Simulation Setup

We consider an MC-CDMA system operating at a carrier of 1.9 GHz with a maximum bandwidth of 5 MHz. We select a frequency offset Δf of 200 Hz, the maximum error tolerated by the 3G standards[12] ($\equiv 0.1$ ppm) for the frequency mismatch between the mobile and the base station [25]. We assume a frequency-selective Rayleigh fading channel with $P^u = P$ propagation paths with exponentially decreasing powers. The channel is correlated across subcarriers and is varying in time with Doppler shift f_D. We suppose a low-Doppler situation $f_D = 8.8$ Hz, unless otherwise mentioned. We consider that the time delays linearly vary in time with a delay drift of 0.049 ppm. The receiver has $M = 2$ antennas. We implement closed-loop power control operating at 1600 Hz and adjusting the power in steps of ± 0.25 dB. An error rate on the power-control bit of 5% and a feedback delay of 0.625 ms are simulated. The simulation parameters common to all the multicarrier-system configurations are listed in Table II.

Table III shows the parameters specific to each MC-CDMA configuration. We choose, as a reference, the 3G DS-CDMA ($N_c = 1$) system with the spreading factor $L = 32$ and a chip rate of 3.84 MHz. We assume frequency-selective fading with $P = 3$ propagation paths. One of the features of the MT-CDMA is that for a constant bandwidth, the ratio between the spreading factor L and $2K = N_c - 1$ is constant. We hence maintain the same chip rate (3.840 MHz) by changing the spreading factor and the number of subcarriers, as shown in Fig. 2. We consider four MT-CDMA configurations. Since they

use the same chip rate, there are three paths in each MT-CDMA subcarrier. For a fair comparison among the different configurations of the MC-DS-CDMA, the bandwidth should be the same. By reducing the chip rate, we varied the number of subcarriers while maintaining the orthogonality between them, as shown in Fig. 2. Due to the reduction in bandwidth, each subcarrier in the MC-DS-CDMA has either two paths (i.e., $P = 2$) or one path (i.e., $P = 1$, frequency-nonselective fading) for $N_c = 3$ and $N_c \geq 5$, respectively. The main performance criterion is the link-level SNR required per carrier to meet a BER of 5% in order to achieve a QoS of BER $= 10^{-6}$ after channel decoding and the resulting system-level throughput. The user's data rate is calculated by summing the data rates over all the subcarriers.

B. Validation of the Performance Analysis

In this section, we investigate the accuracy of the analytical performance analysis in Section III-B under realistic channel conditions. Indeed, we do not assume a perfect channel identification; instead, we use the channel estimate provided by the MC-STAR [13]. We validate the GA of the residual interference by comparison with the simulation results. Since the SUB (Ω) is not explicitly known in this case, it has been obtained from extensive simulations. We consider the following two configurations: DBPSK MT-CDMA ($L = 64$ and $N_c = 3$) and DBPSK MC-DS-CDMA ($L = 32$ and $N_c = 3$). Fig. 4 shows the link-level performances. It is seen, not surprisingly, that the GA is accurate in the presence of a moderate background noise. The accuracy of the GA increases at larger loads or at lower Doppler situations (speed of $V = 5$ km/h). Despite the realistic channel model employed and the channel-estimate errors, there is a very good match between the analytical and simulation results for both the MT-CDMA and the MC-DS-CDMA in the target BER region (5%). This suggests that the analytical evaluation is accurate in a low-Doppler situation.

C. Advantage of Full Interference Suppression

The imperfect frequency downconversion due to the instability of the local oscillators combined with the multipath

TABLE III
PARAMETERS OF EACH MULTICARRIER-SYSTEM CONFIGURATION

Parameter	DS-CDMA	MT-CDMA					MC-DS-CDMA					Comment
λ	-	1					L					subcarrier spacing parameter
N_c	1	3	5	7	9	11	3	5	7	9	11	number of subcarriers
L	32	64	128	192	256	320	32	32	32	32	32	spreading factor
R_c in Mcps	3.840	3.840					1.4549	0.8975	0.6488	0.5081	0.4175	chip rate
P	3	3					2	1	1	1	1	number of paths per subcarrier
R_s in kbaud	120	180	150	140	135	132	136.4	140.2	141.9	142.9	143.5	symbol rate over all subcarriers
R_b for DBPSK in kbps	120	180	150	140	135	132	136.4	140.2	141.9	142.9	143.5	peak rate for DBPSK
R_b for D8PSK in kbps	360	540	450	420	405	396	409.2	420.6	425.7	428.7	430.5	peak rate for D8PSK
BW_{nor}	1	1.026					1					bandwidth normalized vs. DS-CDMA
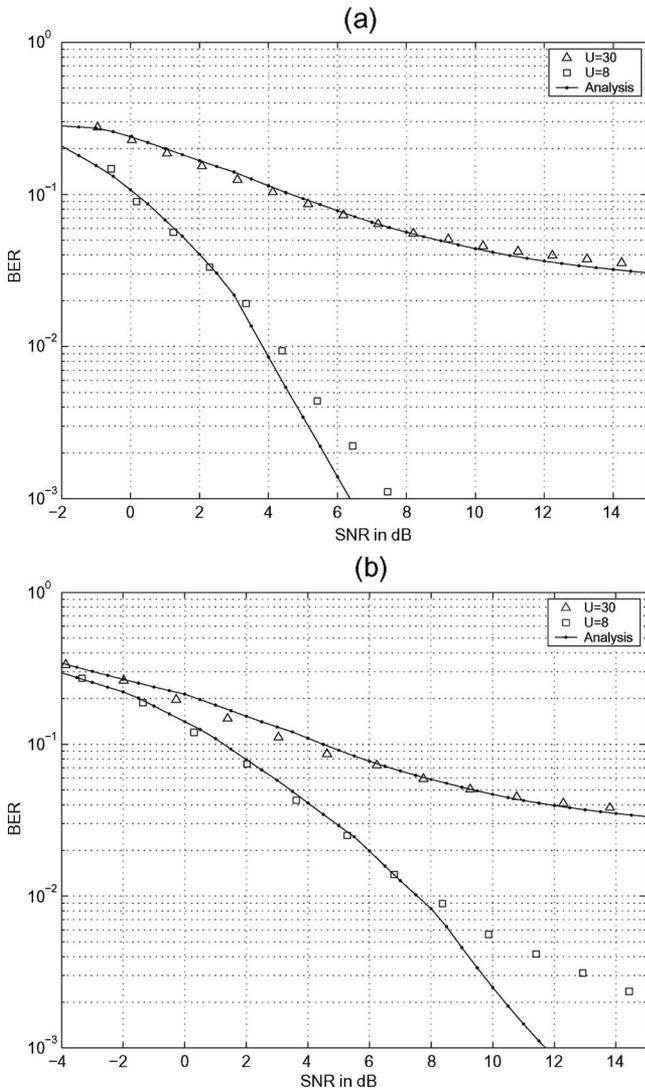
Fig. 4. Analytical and simulated BER of the MC-ISR versus SNR in decibels for (a) MT-CDMA, $L = 64$, $N_c = 3$, and DBPSK and (b) MC-DS-CDMA $L = 32$, $N_c = 3$, and DBPSK.

effect destructs the subcarriers' orthogonality and, hence, causes the ICI. In this section, we evaluate the advantage of full interference suppression on the link-level performance of the MC-CDMA. We show the link-level performance of the MT-CDMA ($L = 64$, $N_c = 3$, and $C = 8$) and the MC-DS-CDMA ($L = 32$, $N_c = 3$, and $C = 8$) with both the MC-MRC (i.e., multicarrier receiver with MRC combining) and the MC-ISR in Fig. 5. It is clear that the MC-ISR performs better than the MC-MRC. Indeed, in low Doppler (speed of $V = 5$ km/h), we report 1.85- and 2-dB gains in SNR for the MT-CDMA and MC-DS-CDMA, respectively. Note that the SNR gains are more important in high-Doppler situation (speed of $V = 50$ km/h). At a bit-error rate of 5%, the MC-ISR performs 5.5 and 3 dB better than the MC-MRC for the MT-CDMA and MC-DS-CDMA, respectively.

In order to evaluate the specific impact of the ICI on the link-level performance, we compare the BER curves of the MT-CDMA ($L = 64$, $N_c = 3$, and $C = 8$) MC-ISR with and without full interference suppression (i.e., with and without ICI suppression). Fig. 6 shows that the MC-ISR with full interference rejection is required to improve system performance. Indeed, at a bit-error rate of 5%, the MC-ISR with full interference suppression performs 1.2 dB better than the MC-ISR with MAI suppression only. In order to capture in more detail the gains achieved by ICI suppression in the MC-CDMA, we proceed in Fig. 7 with additional comparisons between the link-level BER performances of the MC-ISR and the MC-MRC in a single-user context (i.e., $C = 1$, no MAI, only ICI, and negligible ISI). Starting from the reference situation of Fig. 7(a) with $L = 64$, $N_c = 7$, and the DBSPK where the reported SNR gain due to ICI suppression is about 0.5 dB, the results suggest that ICI suppression is even more advantageous at higher rate transmissions, more so increasingly when we move to the scenarios of Fig. 7(b)–(d), i.e., when we increase the number of carriers to $N_c = 11$ (SNR gain is about 1 dB), reduce the processing gain to $L = 32$ (SNR gain is about 3 dB), or increase the modulation order to D8PSK (SNR gain far exceeds 5 dB if not infinite), respectively. These results further confirm the benefits of the ICI rejection in a full-interference-suppression scheme using the MC-ISR.[13]

---

[13]Simulation results that were performed in the framework of this contribution and reported in [14] show that the ICI rejection is even more beneficial in the case of one receiving antenna ($M = 1$).
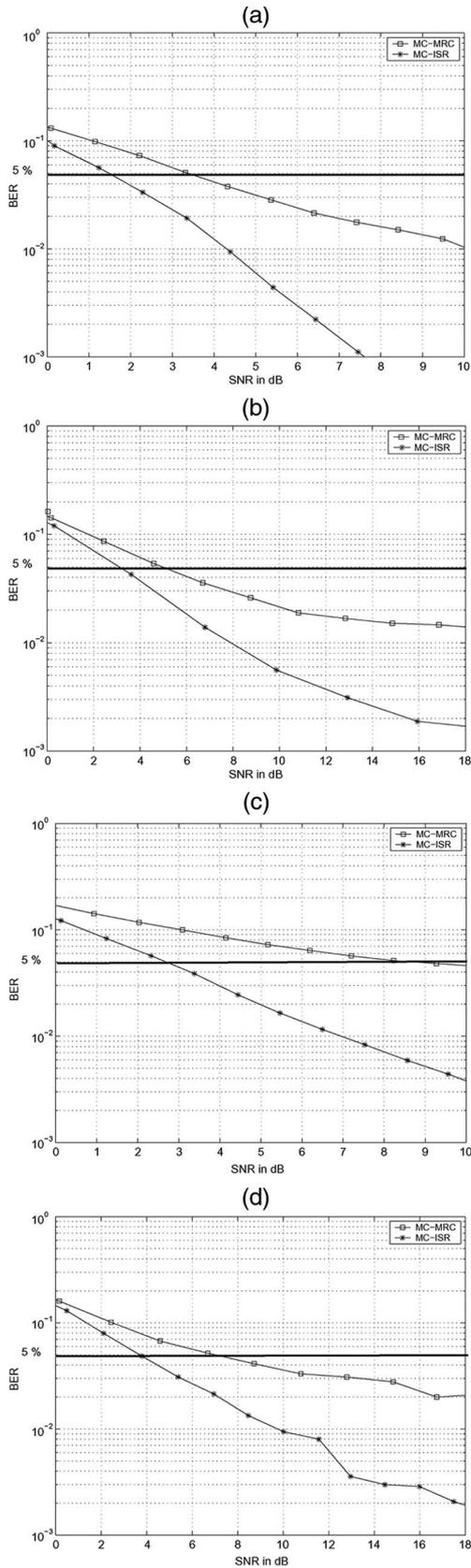
Fig. 5. BER versus SNR in decibels of the MC-MRC and MC-ISR with (a) MT-CDMA, $L = 64$, $N_c = 3$, $C = 8$, DBPSK, and $V = 5$ km/h; (b) MC-DS-CDMA, $L = 32$, $N_c = 3$, $C = 8$, DBPSK, and $V = 5$ km/h; (c) MT-CDMA, $L = 64$, $N_c = 3$, $C = 8$, DBPSK, and $V = 50$ km/h; and (d) MC-DS-CDMA, $L = 32$, $N_c = 3$, $C = 8$, DBPSK, and $V = 50$ km/h.
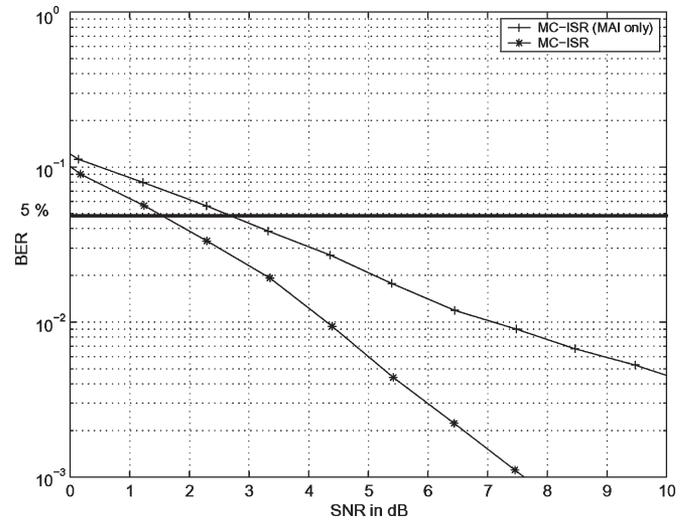
Fig. 6. BER versus SNR in decibels of the MT-CDMA MC-ISR, $L = 64$, $N_c = 3$, and $C = 8$, with and without full interference suppression (i.e., with and without the ICI suppression).

D. MT-CDMA, MC-DS-CDMA, and DS-CDMA Performance Comparison

This section is dedicated to the performance comparison of the proposed MC-ISR receiver with the following two potential next-generation MC-CDMA air-interface configurations: the MT-CDMA and the MC-DS-CDMA. Single-carrier ISR [11] for 3G DS-CDMA air interface is also considered as a reference. In addition, in order to provide a more detailed picture of the aggregate gain of the proposed MC-ISR receiver, we also compared its performance versus the MC-MRC over the same two MC-CDMA air-interface configurations and versus the single-carrier MRC over the current 3G DS-CDMA. First, we derive the SNR_{req} from the link-level simulations. Then, we translate the link-level results into the system-level results using the procedure in Table I. In Table IV, we provide the required SNR and the total throughput of the DBPSK- and D8PSK-modulated data for the DS-CDMA, MT-CDMA, and MC-DS-CDMA. For the DBPSK modulation, we observe that we can improve the system performance by increasing the number of subcarriers. Indeed, the total throughput continues to increase despite the increase in the number of carriers, but a gain saturation is encountered as the number of subcarriers increases. Note, however, that the throughput increase is more important with the MC-ISR due to ICI suppression. Table IV also shows that the MT-CDMA outperforms the MC-DS-CDMA with the DBPSK modulation because it uses longer spreading sequences and that it exploits the subcarrier correlation. Moreover, due to the reduced subcarrier bandwidth, the MC-DS-CDMA has less frequency diversity, whereas the MT-CDMA is better able to exploit path diversity and, hence, achieves better performance. Note also that the MC-DS-CDMA is more robust against the ICI, but, in applying the MC-ISR, this advantage over the MT-CDMA becomes obsolete, and the performance gap between the MT-CDMA and MC-DS-CDMA increases.

Next, we compare the different configurations with the D8PSK modulation. We notice a link-level deterioration for
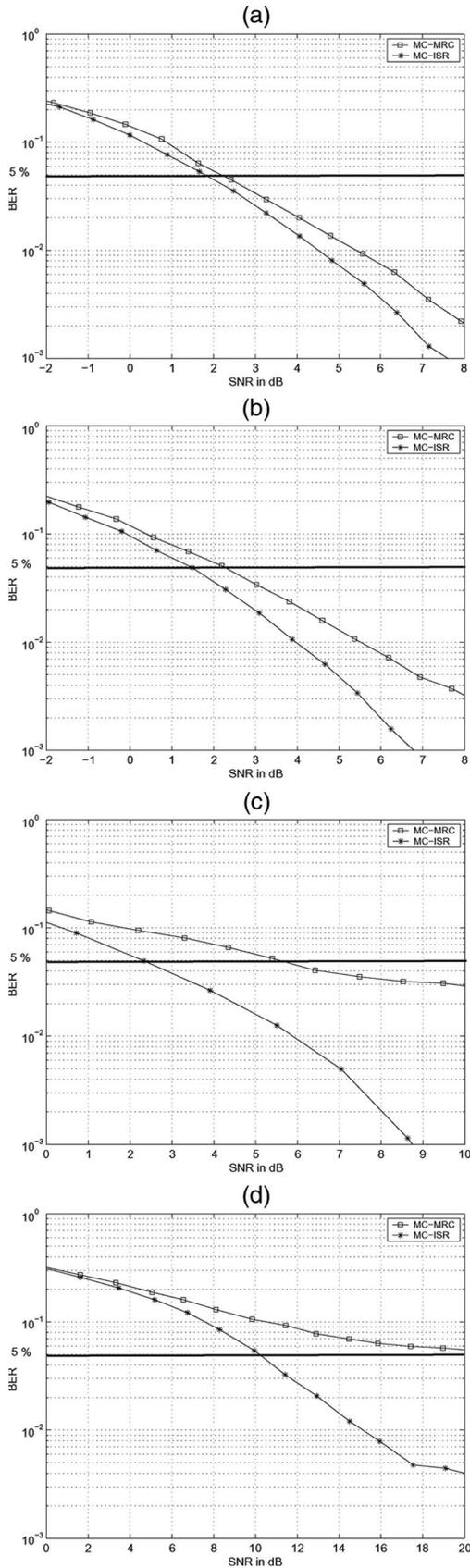
Fig. 7. BER versus SNR in decibels of the MC-ISR and MC-MRC with single-user MT-CDMA and (a) $L = 64$, $N_c = 7$, and DBPSK; (b) $L = 64$, $N_c = 11$, and DBPSK; (c) $L = 32$, $N_c = 7$, and DBPSK; and (d) $L = 64$, $N_c = 7$, and D8PSK.

the MT-CDMA as the number of subcarriers increases. Indeed, a higher order modulation is more sensitive to the residual ICI. The MC-DS-CDMA is much less affected by this phenomenon because it is much more robust to the ICI, owing to the higher subcarrier spacing. Therefore, with a high-order modulation, the MC-DS-CDMA outperforms the MT-CDMA when the number of subcarriers is high enough. We notice also that, with the MC-MRC combiner, the D8PSK MC-DS-CDMA outperforms the D8PSK MT-CDMA, even with a small number of subcarriers. It is clear, however, that the D8PSK is less efficient than the DBPSK modulation for all air-interface configurations. In Table IV, we highlight the most spectrum-efficient MC-ISR air-interface configuration for each modulation. For both modulations, the MT-CDMA has the best link-level performance and the highest throughput (for a tested number of carriers less than or equal to 11). The MT-CDMA with nine subcarriers and DBPSK modulation outperforms all the other configurations and provides a throughput about 115% higher than that achievable with the single-carrier MRC over a 3G DS-CDMA air interface. The net benefits due to the proposed MC-ISR combiner and to the potential migration to a next-generation MT-CDMA air interface are about 80 and 15%, respectively.

V. CONCLUSION

In this contribution, we proposed a spectrum-efficient low-complexity MC-CDMA space–time receiver with full-interference-suppression capabilities named the MC-ISR. First, we derived a complete model of the interference, which takes into account the MAI, the ISI, and the ICI in a multipath fading channel with a timing and frequency mismatch. Based on this model, we proposed a new MC-ISR receiver. We incorporated the least complex and the more practical ISR interference-rejection mode to simultaneously suppress the MAI, the ISI, and the ICI at the signal-combining step. We also proposed a realistic implementation of the new MC-ISR receiver, which includes an efficient strategy for carrier-offset recovery in a multicarrier- and multiuser-detection scheme. The MC-ISR supports both the MT-CDMA and the MC-DS-CDMA air interfaces. Furthermore, the assessment of the new MC-ISR receiver was oriented toward an implementation in a future real-world wireless system. Indeed, we analyzed the performance of the MC-ISR in an unknown time-varying Rayleigh channel with multipath, carrier offset, and cross correlation between subcarrier channels and took into account all the channel-estimation errors. As another contribution in this paper, we derived a link-/system-level performance analysis of the MC-ISR based on the GA and validated it by simulations. Under realistic propagation conditions and in the presence of channel-estimation errors, the simulation results validated the performance analysis and confirmed the net advantage of the full-interference-suppression capabilities of the MC-ISR. With two receiving antennas and nine MT-CDMA subcarriers in a 5-MHz bandwidth, the MC-ISR provides about 4320 kb/s at low mobility for the DBPSK, i.e., an increase of 115% in the throughput over the current 3G DS-CDMA with an MRC.

TABLE IV
REQUIRED SNR AND MAXIMUM THROUGHPUT OF DS-CDMA, MT-CDMA, AND MC-DS-CDMA FOR DBPSK AND D8PSK
(BEST PERFORMANCE VALUES FOR EACH MODULATION ARE IN BOLD)

MC-STAR configuration	DS-CDMA	MT-CDMA					MC-DS-CDMA				
N_c	1	3	5	7	9	11	3	5	7	9	11
Modulation	DBPSK										
SNR_{req} in dB with MC-MRC	0.76	0.74	0.76	0.59	0.57	0.69	3.7	2.8	2.7	2.55	3
$\mathcal{T}_{max}$ in kbps with MC-MRC	2040	2160	2100	2240	2295	2244	1091.2	1402	1419	1571.9	1435
SNR_{req} in dB with MC-ISR	0.76	0.74	0.75	0.55	**0.5**	0.62	3.62	2.8	2.6	2.48	3
$\mathcal{T}_{max}$ in kbps with MC-ISR	3600	3960	4050	4200	**4320**	4224	2182.4	2523.6	2554.2	2572.2	2439.5
Modulation	D8PSK										
SNR_{req} in dB with MC-MRC	8.57	8	9.28	9	10	11	11	10.25	10.34	10.05	10.8
$\mathcal{T}_{max}$ in kbps with MC-MRC	1080	1080	900	840	810	792	818.4	841.2	851.4	857.4	861
SNR_{req} in dB with MC-ISR	8.57	**7.86**	8.8	8.9	9.4	10.5	10.94	10.25	10.2	10.02	10.8
$\mathcal{T}_{max}$ in kbps with MC-ISR	1800	**2160**	1350	1260	1215	792	1227.6	1261.8	1277.1	1286.1	861

APPENDIX

Derivation of the Interference Variance After MC-ISR Combining

Our goal is to estimate the variances

$$
\mathrm{Var}\left[\delta^d_{\mathrm{MAI},k,n} + \delta^d_{\mathrm{ICI},k,n} + \delta^d_{\mathrm{ISI},k,n}\right]
$$

$$
= \mathrm{Var}\Bigg[\sum_{\substack{u=1 \\ u\neq d}}^{C} \sum_{k'=-K}^{K} \sum_{n'=n-1}^{n+1} \xi^u_{k',n'} \lambda^u_{k',n} \underline{W}^{d\mathrm{H}}_{k,n} \underline{\widehat{Y}}^u_{n',k',n}
$$

$$
+ \sum_{\substack{k'=-K \\ k'\neq k}}^{K} \sum_{n'=n-1}^{n+1} \xi^d_{k',n'} \lambda^d_{k',n} \underline{W}^{d\mathrm{H}}_{k,n} \underline{\widehat{Y}}^d_{n',k',n}
$$

$$
+ \sum_{\substack{n'=n-1 \\ n'\neq n}}^{n+1} \xi^d_{k,n'} \lambda^d_{k,n} \underline{W}^{d\mathrm{H}}_{k,n} \underline{\widehat{Y}}^d_{n',k,n} \Bigg]. \tag{53}
$$

Let us consider the general problem of deriving the variance of the sum of random complex variables. We first introduce the variables x_α, $\alpha \in \{1,\ldots,N_T\}$ and ξ_α, $\alpha \in \{1,\ldots,N_T\}$ with the following properties: $E[\xi_\alpha \xi^*_{\alpha'}] = M_\xi$, $\forall \alpha \neq \alpha'$, $E[\xi_\alpha \xi^*_\alpha] = V_\xi$, $E[x_\alpha] = 0$, and $\mathrm{Var}[\sum_{\alpha=1}^{N_T} x_\alpha] = 0$. Then, we assume that ξ_α and x_α are independent. Thus, we derive the variance as follows:

$$
\mathrm{Var}\left[\sum_{\alpha=1}^{N_t} \xi_\alpha x_\alpha \right]
$$

$$
= \sum_{\alpha=1}^{N_t} \mathrm{Var}[\xi_\alpha x_\alpha] + \sum_{\alpha=1}^{N_t} \sum_{\substack{\alpha'=1 \\ \alpha'\neq\alpha}}^{N_t} E[\xi_\alpha \xi_{\alpha'} x_\alpha x_{\alpha'}]
$$

$$
= \sum_{\alpha=1}^{N_t} V_\xi \mathrm{Var}[x_\alpha] + \sum_{\alpha=1}^{N_t} \sum_{\substack{\alpha'=1 \\ \alpha'\neq\alpha}}^{N_t} E[\xi_\alpha \xi_{\alpha'}] E[x_\alpha x_{\alpha'}]
$$

$$
= \sum_{\alpha=1}^{N_t} V_\xi \mathrm{Var}[x_\alpha] + \sum_{\alpha=1}^{N_t} \sum_{\substack{\alpha'=1 \\ \alpha'\neq\alpha}}^{N_t} \rho_\xi E[x_\alpha x_{\alpha'}]. \tag{54}
$$

From $\mathrm{Var}[\sum_{\alpha=1}^{N_T} x_\alpha] = 0$, we have

$$
\mathrm{Var}\left[\sum_{\alpha=1}^{N_t} x_\alpha \right] = \sum_{\alpha=1}^{N_t} \mathrm{Var}[x_\alpha] + \sum_{\alpha=1}^{N_t} \sum_{\substack{\alpha'=1 \\ \alpha'\neq\alpha}}^{N_t} E[x_\alpha x_{\alpha'}] = 0
$$

$$
\Rightarrow \sum_{\alpha=1}^{N_t} \sum_{\substack{\alpha'=1 \\ \alpha'\neq\alpha}}^{N_t} E[x_\alpha x_{\alpha'}] = - \sum_{\alpha=1}^{N_t} \mathrm{Var}[x_\alpha]. \tag{55}
$$

Then, by replacing (55) into (54), we obtain

$$
\mathrm{Var}\left[\sum_{\alpha=1}^{N_t} \xi_\alpha x_\alpha \right] = (V_\xi - \rho_\xi) \sum_{\alpha=1}^{N_t} \mathrm{Var}[x_\alpha]. \tag{56}
$$

Now, we apply the same procedure to derive the variance of $\delta^d_{\mathrm{MAI},k,n} + \delta^d_{\mathrm{ICI},k,n} + \delta^d_{\mathrm{ISI},k,n}$. We substitute ξ_α by $\xi^u_{k',n'} \lambda^u_{k',n}$ and x_α by $\underline{W}^{d\mathrm{H}}_{k,n} \underline{\widehat{Y}}^u_{n',k',n}$. The MC-ISR combiner $\underline{W}^d_{k,n}$ satisfies the optimization property in (25), and thus

$$
\underline{W}^{d\mathrm{H}}_{k,n} \underline{\widehat{I}}^d_{k,n} = 0
$$
$$
\longrightarrow \mathrm{Var}\left[\underline{W}^{d\mathrm{H}}_{k,n} \left(\underline{\widehat{I}}^d_{\mathrm{MAI},k,n} + \underline{\widehat{I}}^d_{\mathrm{ICI},k,n} + \underline{\widehat{I}}^d_{\mathrm{ISI},k,n} \right) \right] = 0. \tag{57}
$$

Then

$$
\mathrm{Var}\left[\delta^d_{\mathrm{MAI},k,n} + \delta^d_{\mathrm{ICI},k,n} + \delta^d_{\mathrm{ISI},k,n} \right]
$$

$$
= (V_\xi - \rho_\xi) \sum_{\substack{u=1 \\ u\neq d}}^{C} \sum_{k'=-K}^{K} \sum_{n'=n-1}^{n+1} \mathrm{Var}\left[\underline{W}^{d\mathrm{H}}_{k,n} \underline{\widehat{Y}}^u_{n',k',n} \right]
$$

$$
+ (V_\xi - \rho_\xi) \sum_{\substack{k'=-K \\ k'\neq k}}^{K} \sum_{n'=n-1}^{n+1} \mathrm{Var}\left[\underline{W}^{d\mathrm{H}}_{k,n} \underline{\widehat{Y}}^d_{n',k',n} \right]
$$

$$
+ (V_\xi - \rho_\xi) \sum_{\substack{n'=n-1 \\ n'\neq n}}^{n+1} \mathrm{Var}\left[\underline{W}^{d\mathrm{H}}_{k,n} \underline{\widehat{Y}}^d_{n',k,n} \right]. \tag{58}
$$

We consider that $E[\|\underline{W}^d_{k,n}\|^2] = \overline{\kappa}$, which is a measure of the enhancement of the white noise compared to the MRC combiner [21]. We also assume that the combiner $\underline{W}^d_{k,n}$ and

the $\widehat{\underline{Y}}^u_{n',k',n}$ are uncorrelated. Thus, we derive the variance of the residual interference as follows:

$$
\begin{aligned}
&\mathrm{Var}\left[\delta^d_{\mathrm{MAI},k,n} + \delta^d_{\mathrm{ICI},k,n} + \delta^d_{\mathrm{ISI},k,n}\right] \\
&= (V_\xi - \rho_\xi)\overline{\kappa}\sum_{\substack{u=1\\u\neq d}}^{C}\sum_{k'=-K}^{K}\sum_{n'=n-1}^{n+1}\mathrm{Var}\left[\widehat{\underline{Y}}^u_{n',k',n}\right] \\
&\quad + (V_\xi - \rho_\xi)\overline{\kappa}\sum_{\substack{k'=-K\\k'\neq k}}^{K}\sum_{n'=n-1}^{n+1}\mathrm{Var}\left[\widehat{\underline{Y}}^d_{n',k',n}\right] \\
&\quad + (V_\xi - \rho_\xi)\overline{\kappa}\sum_{\substack{n'=n-1\\n'\neq n}}^{n+1}\mathrm{Var}\left[\widehat{\underline{Y}}^d_{n',k,n}\right] \\
&= (V_\xi - \rho_\xi)\overline{\kappa}\mathrm{Var}\left[\widehat{\underline{I}}^d_{k,n}\right].
\end{aligned}
\tag{59}
$$

In the developments of (59), we exploited the fact that we transmit different data sequences over distinct subcarriers for a given user and, hence, assumed that the cross-correlation terms from different subcarriers are zero. In the following, we will derive the value of V_ξ and ρ_ξ under the following three assumptions: 1) The error-indicating variables $\xi^u_{k',n'}$ and $\lambda^u_{k',n}$ are independent. 2) All the random-sequence variables $(\xi^u_{k',n'})$ and $(\lambda^u_{k',n})$ are independent and identically distributed. 3) $E[\lambda^u_{k',n}] = 1$. Given these assumptions, we derive V_ξ as follows:

$$
\begin{aligned}
V_\xi &= E\left[\xi^u_{k',n'}\lambda^u_{k',n}\xi^{u*}_{k',n'}\lambda^{u*}_{k',n}\right] \\
&= E\left[\xi^u_{k',n'}\xi^{u*}_{k',n'}\right]E\left[\lambda^u_{k',n}\lambda^{u*}_{k',n}\right] \\
&= E\left[\lambda^u_{k',n}\lambda^{u*}_{k',n}\right] \\
&= [1 + \rho_\lambda].
\end{aligned}
\tag{60}
$$

In order to evaluate V_ξ, we exploit the expression of the variance of the power-control error in [26]. Hence, ρ_λ varies with the maximum Doppler frequency f_D in [26, eq. (51)], yielding

$$
\rho_\lambda = \frac{4\pi^2(f_D \times \tau_{\mathrm{PC}})^2}{P-1}
\tag{61}
$$

where τ_{PC} is the power-control feedback delay. Next, we derive the expectation $\rho_\xi = E[\xi^u_{k',n'}\lambda^u_{k',n}\xi^{u'*}_{k',n'}\lambda^{u'*}_{k',n}] = E[\xi^u_{k',n'}]E[\xi^{u'*}_{k',n'}]E[\lambda^u_{k',n}]E[\lambda^{u'*}_{k',n}] = E[\xi^u_{k',n'}]^2$. If $S_{\mathrm{rec}} \ll 1$, the value of ρ_ξ can be derived as follows [21]:

$$
\rho_\xi \simeq \left(1 - (1-\cos(2\pi/\mathcal{M}_i))\,S_{\mathrm{rec}}\right)^2.
\tag{62}
$$

The interference $\underline{I}^d_{k,n}$ is approximated as a Gaussian distributed random variable with a zero mean. Only its variance needs to be evaluated to derive the variance of the residual interference in (59).

Derivation of the Interference Variance for Band-Limited MC-CDMA

The chip waveform has been noted to be an important system parameter for the DS-CDMA and MC-DS-CDMA. Hence, the performance of the DS-CDMA and MC-DS-CDMA with various time-limited and band-limited chip waveforms have been investigated. However, for all the MT-CDMA systems found in the literature, a time-limited waveform is generally employed [1], [27]–[29]. Since we consider a practical square-root-raised-cosine pulse, the focus of this Appendix is to derive the variance of the interference of the MC-CDMA (including the MC-DS-CDMA and MT-CDMA) with a band-limited square-root-raised-cosine waveform. Let $G(f)$ be the Fourier transform of the raised-cosine filter, shown in (63) at the bottom of the page. Let $\overline{\psi^2_D} = E[(\psi^d_k)^2]$ be the average power of the kth carrier of the desired user and $\overline{\psi^2_I}$ be the average power on each interfering carrier (assumed equal for all u and all k). Using the general results in [30], one has

$$
\mathrm{Var}\left[\underline{I}^d_{\mathrm{MAI},k,n}\right] = (C-1)\frac{\overline{\psi^2_I}}{L}[\varsigma(\beta) + \chi_k(\beta)]
\tag{64}
$$

where

$$
\varsigma(\beta) = \frac{1}{T_c}\int_{-\infty}^{\infty}G^2(f)\,df
\tag{65}
$$

and

$$
\chi_k(\beta) = \sum_{\substack{k'=-K\\k'\neq k}}^{K}\frac{1}{T_c}\int_{-\infty}^{\infty}G(f)G\left(f-(f_k-f_{k'})\right)\,df.
\tag{66}
$$

It is easy to obtain $\varsigma(\beta) = (1-(\beta/4))$. To obtain $\chi_k(\beta)$, we need to separately consider the MC-DS-CDMA and MT-CDMA systems. After mathematical evaluations of the integral, we obtain

$$
\chi_k(\beta) = \begin{cases} \frac{\beta}{8}, & \text{if } k = -K \text{ or } K \\ \frac{\beta}{4}, & \text{if } k = -K+1,\ldots,K-1 \end{cases}
\tag{67}
$$

for the MC-DS-CDMA ($\lambda = L$ and $f_k = k/T_c$) and

$$
\chi_k(\beta) = \sum_{\substack{k'=-K\\k'\neq k}}^{K}\vartheta\left(|k-k'|\right)
\tag{68}
$$

where $\vartheta(x)$ is defined in (38) for the MT-CDMA ($\lambda = 1$ and $f_k = k/T_{\mathrm{MC}}$). The variances of the residual ICI and ISI

$$
G(f) = \begin{cases} T_c, & 0 \leq |f| \leq \frac{1-\beta}{2T_c} \\ \frac{T_c}{2}\left\{1 + \cos\left[\frac{\pi T_c}{\beta}\left(|f| - \frac{1-\beta}{2T_c}\right)\right]\right\}, & \frac{1-\beta}{2T_c} \leq |f| \leq \frac{1+\beta}{2T_c} \\ 0, & |f| > \frac{1+\beta}{2T_c} \end{cases}
\tag{63}
$$

interferences from the same user can be written as

$$\mathrm{Var}\left[\underline{I}_{\mathrm{ICI},k,n}^{d}\right] = \frac{\overline{\psi}_D^2}{L}\delta_{\mathrm{is}}\chi_k(\beta)$$

$$\mathrm{Var}\left[\underline{I}_{\mathrm{ISI},k,n}^{d}\right] = \frac{\overline{\psi}_D^2}{L}\delta_{\mathrm{is}}\varsigma(\beta) \tag{69}$$

where $\delta_{\mathrm{is}} = (P-1)/P$ is a measure of the relative impact of the interference generated by the other paths on a given path of the desired user.

REFERENCES

[1] Y. Lie-Liang and L. Hanzo, "Performance of generalized multicarrier DS-CDMA over Nakagami-m fading channels," *IEEE Trans. Commun.*, vol. 50, no. 6, pp. 956–966, Jun. 2002.
[2] H. Steendam and M. Moeneclaey, "The effect of carrier frequency offsets on downlink and uplink MC-DS-CDMA," *IEEE J. Sel. Areas Commun.*, vol. 19, no. 12, pp. 2528–2536, Dec. 2001.
[3] X. Weiping and L. B. Milstein, "MMSE interference suppression for multicarrier DS-CDMA in frequency selective channels," in *Proc. IEEE GLOBECOM*, 1998, vol. 1, pp. 259–264.
[4] F. Lin and L. B. Milstein, "Successive interference cancellation in multicarrier DS/CDMA," *IEEE Trans. Commun.*, vol. 48, no. 9, pp. 1530–1540, Sep. 2000.
[5] W. Huahui, K. W. Ang, K. Yen, and Y. H. Chew, "An adaptive PIC receiver with diversity combining for MC-DS-CDMA system," in *Proc. IEEE VTC—Fall*, 2003, vol. 2, pp. 1055–1059.
[6] W. Huahui, K. W. Ang, K. Yen, and Y. H. Chew, "Performance analysis of an adaptive PIC receiver for asynchronous multicarrier DS-CDMA system," in *Proc. IEEE PIMRC*, 2003, vol. 2, pp. 1835–1839.
[7] H. Lie-Liang, H. Wei, and L. Hanzo, "Multiuser detection in multicarrier CDMA systems employing both time-domain and frequency-domain spreading," in *Proc. IEEE PIMRC*, 2003, vol. 2, pp. 1840–1844.
[8] W. Nabhane and H. V. Poor, "Blind joint equalization and multiuser detection in dispersive MC-CDMA/MC-DS-CDMA/MT-CDMA channels," in *Proc. IEEE MILCOM*, 2002, vol. 2, pp. 814–819.
[9] J. Namgoong, T. F. Wong, and J. S. Lehnert, "Subspace multiuser detection for multicarrier DS-CDMA," *IEEE Trans. Commun.*, vol. 48, no. 11, pp. 1897–1908, Nov. 2000.
[10] M. Peng, Y. J. Guo, and S. K. Barton, "Multiuser detection of asynchronous CDMA with frequency offset," *IEEE Trans. Commun.*, vol. 49, no. 6, pp. 952–960, Jun. 2001.
[11] S. Affes, H. Hansen, and P. Mermelstein, "Interference subspace rejection: A framework for multiuser detection in wideband CDMA," *IEEE J. Sel. Areas Commun.*, vol. 20, no. 2, pp. 287–302, Feb. 2002.
[12] S. Affes and P. Mermelstein, "Adaptive space–time processing for wireless CDMA," in *Adaptive Signal Processing: Application to Real-World Problems*, J. Benesty and A. H. Huang, Eds. Berlin, Germany: Springer-Verlag, Jan. 2003.
[13] B. Smida, S. Affes, J. Li, and P. Mermelstein, "Multicarrier-CDMA STAR with time and frequency synchronization," in *Proc. IEEE ICC*, 2005, vol. 4, pp. 2493–2499.
[14] B. Smida, S. Affes, K. Jamaoui, and P. Mermelstein, "A multicarrier-CDMA receiver with full interference suppression and carrier frequency offset recovery," in *Proc. IEEE SPAWC*, Jun. 2005, pp. 435–439.
[15] 3GPP TR 101 112 V3.1.0, *Universal Mobile Telecommunications System (UMTS); Selection Procedures for the Choice of Radio Transmission Technologies of the UMTS*, Nov. 1997.
[16] S. Affes, D. Feng, L. Ge, and P. Mermelstein, "Does direction-of-arrival estimation help channel identification in multi-antenna CDMA receivers?" in *Proc. IEEE ISWC*, 2002, pp. 167–168. Invited Paper.
[17] *Microwave Mobile Communications*, W. C. Jakes, Ed. New York: Wiley, 1974.
[18] B. Natarajan, C. R. Nassar, and V. Chandrasekhar, "Generation of correlated Rayleigh fading envelopes for spread spectrum applications," *IEEE Commun. Lett.*, vol. 4, no. 1, pp. 9–11, Jan. 2000.
[19] R. B. Ertel and J. H. Reed, "Generation of two equal power correlated Rayleigh fading envelopes," *IEEE Commun. Lett.*, vol. 2, no. 10, pp. 276–278, Oct. 1998.
[20] S. Affes and P. Mermelstein, "A new receiver structure for asynchronous CDMA: STAR the spatio-temporal array-receiver," *IEEE J. Sel. Areas Commun.*, vol. 16, no. 8, pp. 1411–1422, Oct. 1998.
[21] H. Hansen, S. Affes, and P. Mermelstein, "Mathematical derivation of interference subspace rejection," Montreal, QC, Canada, Tech. Rep., INRS-EMT, EMT-014-0105, Jan. 2005.
[22] B. Smida and S. Affes, "On the performance of interference subspace rejection for next generation multicarrier CDMA," in *Proc. IEEE ISSPA*, Aug. 2005, pp. 415–418.
[23] T. S. Rappaport, *Wireless Commmunications: Principles & Practice*. Englewood Cliffs, NJ: Prentice-Hall, 1999.
[24] B. Smida, S. Affes, and P. Mermelstein, "Joint time-delay and frequency offset synchronization for CDMA array-receivers," in *Proc. IEEE SPAWC*, 2003, pp. 499–504.
[25] 3GPP TS 25.101 V5.4.0, *3rd Generation Partnership Project (3GPP), Technical Specification Group (TSG), Radio Access Network (RAN), UE Radio Transmission and Reception (FDD)*, Sep. 2002.
[26] A. Abrardo and D. Sennati, "On the analytical evaluation of closed-loop power-control error statistics in DS-CDMA cellular systems," *IEEE Trans. Veh. Technol.*, vol. 49, no. 6, pp. 2071–2080, Nov. 2000.
[27] Y. Lie-Liang and L. Hanzo, "Performance of generalized multicarrier DS-CDMA using various chip waveforms," *IEEE Trans. Commun.*, vol. 51, no. 5, pp. 748–752, May 2003.
[28] L. Vandendorpe, "Multitone spread spectrum multiple access communications system in a multipath Rician fading channel," *IEEE Trans. Veh. Technol.*, vol. 44, no. 2, pp. 327–337, May 1995.
[29] Q. M. Rahman and A. B. Sesay, "Performance analysis of MT-CDMA system with diversity combining," in *Proc. IEEE MILCOM*, 2001, vol. 2, pp. 1360–1364.
[30] S. Kondo and B. Milstein, "Performance of multicarrier DS CDMA systems," *IEEE Trans. Commun.*, vol. 44, no. 2, pp. 238–246, Feb. 1996.

Besma Smida (S'98–M'06) received the Dipl.Ing. degree in telecommunications from École Supérieure des Communications de Tunis, Ariana, Tunisia, in 1995 and the M.Sc. and Ph.D. degrees in telecommunications from the Institut National de la Recherche Scientifique, Centre Energie, Matériaux, et Télécommunications (INRS-EMT), University of Quebec, Montreal, QC, Canada, in 1998 and 2006, respectively.

From 1998 to 1999, she was a Research Assistant with the Personal Communications Group, INRS-EMT. From 1999 to 2002, she was a Research Engineer with the Technology Evolution and Standards Group, Microcell Solutions, Montreal, surveying and studying radio-communication-technology evolution. She also took part in major wireless normalization committees (3GPP and T1P1). She is currently a Postdoctorate Fellow with the School of Engineering and Applied Sciences, Harvard University, Cambridge, MA. Her current research interests include multicarrier modulation, spread spectrum, and network-aware application.

Sofiène Affes (S'94–M'95–SM'04) received the Dipl.Ing. degree in electrical engineering and the Ph.D. degree (with honors) in signal processing from the École Nationale Supérieure des Télécommunications, Paris, France, in 1992 and 1995, respectively.

He has been with the Institut National de la Recherche Scientifique, Centre Energie, Matériaux, et Télécommunications (INRS-EMT), University of Quebec, Montreal, QC, Canada, as a Research Associate from 1995 to 1997 and then as an Assistant Professor until 2000. Currently, he is an Associate Professor with the Wireless Communications Group, INRS-EMT, University of Quebec. From 1998 to 2002, he was the Bell/Nortel/Natural Sciences and Engineering Research Council (NSERC) Industrial Research Chair in Personal Communications, INRS-EMT, University of Quebec, where he led the radio-design and signal processing activities. Currently, he holds a Canada Research Chair in High-Speed Wireless Communications. He is currently actively involved in a major project in wireless of the Partnerships for Research on Microelectronics, Photonics, and Telecommunications—Québec. His research interests are in wireless communications, statistical signal and array processing, adaptive space–time processing, and multiple-input multiple-output technology.

Dr. Affes is the corecipient of the 2002 Prize for Research Excellence of INRS. He served as the General Cochair of the 2006 IEEE Vehicular Technology Fall Conference and is currently a member of the Editorial Board of the *Wiley Journal on Wireless Communications and Mobile Computing*.

Kamal Jamaoui received the Computer Science Engineering degree (Ing.) from the Ecole Polytechnique de Montreal, Montreal, QC, Canada, in 2002 and the M.Sc. degree from the Institut National de la Recherche Scientifique, Centre Energie, Matériaux, et Télécommunications, University of Quebec, Montreal.

He is with INSAF EXPERTISE, Casablanca, Morocco, as a Consulting Engineer in the telecommunications and high-tech fields. He is also a Professor/Assistant with l'Ecole Polytechique Privee de Casablanca, Casablanca. His research interests include orthogonal frequency-division multiplexing, multicarrier-code-division-multiple-access receivers with full interference suppression, and wireless networks.
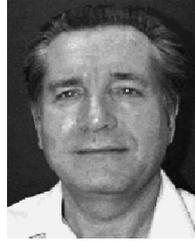
Paul Mermelstein (S'58–M'63–SM'77–F'94) received the B.Eng. degree in engineering physics from McGill University, Montreal, QC, Canada, in 1959 and the S.M., E.E., and D.Sc. degrees in electrical engineering from the Massachusetts Institute of Technology, Cambridge, in 1960, 1963, and 1964, respectively.

From 1964 to 1973, he was a member of the Technical Staff with the Speech and Communications Research Department, Bell Laboratories, Murray Hill, NJ. From 1973 to 1977, he was a member of the Research Staff with the Haskins Laboratories, where he was conducting research on speech analysis, perception, and recognition. From 1977 to 1994, he was with Bell Northern Research, Ottawa, ON, Canada, where he held a variety of management positions leading research and development activities in speech recognition, speech coding, and personal communications. From 1994 to 2000, he was the Leader of the major program in personal and mobile communications of the Canadian Institute for Telecommunications Research. From 1994 to 2003, he was the Bell/Nortel/Natural Sciences and Engineering Research Council Industrial Research Chair in Personal Communications with the Institut National de la Recherche Scientifique, Centre Energie, Matériaux, et Télécommunications, University of Quebec, Montreal, where he is now a Professor Emeritus. Since 2004, he has also been serving as an Adjunct Professor of electrical engineering with the University of Miami, Coral Gables, FL.